J Neurophysiol 109: 1360–1377, 2013.
First published December 5, 2012; doi:10.1152/jn.00577.2012.

A model of cholinergic modulation in olfactory bulb and piriform cortex

Licurgo de Almeida,[1] Marco Idiart,[2] and Christiane Linster[1]

[1]*Department of Neurobiology and Behavior, Cornell University, Ithaca, New York; and* [2]*Physics Institute, UFRGS, Porto Alegre, Brazil*

Submitted 9 July 2012; accepted in final form 28 November 2012

de Almeida L, Idiart M, Linster C. A model of cholinergic modulation in olfactory bulb and piriform cortex. *J Neurophysiol* 109: 1360–1377, 2013. First published December 5, 2012; doi:10.1152/jn.00577.2012.—In this work we investigate in a computational model how cholinergic inputs to the olfactory bulb (OB) and piriform cortex (PC) modulate odor representations. We use experimental data derived from different physiological studies of ACh modulation of the bulbar and cortical circuitry and the interaction between these two areas. The results presented here indicate that cholinergic modulation in the OB significantly increases contrast and synchronization in mitral cell output. Each of these effects is derived from distinct neuronal interactions, with different groups of interneurons playing different roles. Both bulbar modulation effects contribute to more stable learned representations in PC, with pyramidal networks trained with cholinergic-modulated inputs from the bulb exhibiting more robust learning than those trained with unmodulated bulbar inputs. This increased robustness is evidenced as better recovery of memories from corrupted patterns and lower-concentration inputs as well as increased memory capacity.

theoretical model; integrate and fire; neural network; olfaction; acetylcholine

THE OLFACTORY BULB (OB) and piriform cortex (PC) receive cholinergic inputs from the horizontal limb of the diagonal band of Broca (HDB) (Brashear et al. 1986; Zaborszky et al. 1986). Ideas about the function of these projections include *1*) contrast enhancement in the OB (Chaudhury et al. 2009; Cleland and Sethupathy 2006; Linster and Cleland 2002; Mandairon et al. 2006) and *2*) improvement of associative memory function in the PC (Hasselmo et al. 1992; Linster et al. 2003). Both the bulb and cortex are densely interconnected and receive common cholinergic inputs from the HDB. Experimental data show strong modulation of both regions, at the cellular (Castillo et al. 1999; Hasselmo and Bower 1992; Pressler et al. 2007), network (Hasselmo and Barkai 1995; Linster et al. 2003), and perceptual (Chaudhury et al. 2009; Linster et al. 2009) levels.

In the OB, acetylcholine (ACh) modulates periglomerular (PG) and mitral (Mi) cell excitability (Castillo et al. 1999; Chaudhury et al. 2009; Ravel et al. 1990) and granule (Gr) cell afterdepolarization and excitability (Nickell and Shipley 1988; Pressler et al. 2007). Local cholinergic modulation of bulbar function during behavioral assays affects the perceptual discrimination between highly similar odorants (Mandairon et al. 2006); computational models of the known cellular effects show that changes in OB neurons can be sufficient to predict the perceptual effects on odor discrimination (Mandairon et al. 2006). In the PC, ACh modulates the excitability and afterhyperpolarization of pyramidal (Pyr) cells and interneurons (Barkai and Hasselmo 1994; Tseng and Haberly 1989), excitatory synaptic transmission of intrinsic connections (Hasselmo and Bower 1992; Williams and Constanti 1988), as well as synaptic plasticity (Hasselmo and Barkai 1995; Patil et al. 1998). Behaviorally, local cholinergic modulation affects the specificity of odor memory formation in the PC (Linster et al. 2009; Wilson 2001). While computational models also suggest a role for the storage of overlapping odor information, these ideas have only been tested with global injections or lesions of cholinergic neurons in the HDB, which are not specific to the PC (De Rosa and Hasselmo 2000; De Rosa et al. 2001). Lesions of HDB neurons, assumed to decrease cholinergic inputs to both the OB and the PC, decrease discrimination between similar odorants (Linster and Cleland 2002; Linster and Hasselmo 2001; Mandairon et al. 2006) and increase interference between overlapping odor pairs (De Rosa and Hasselmo 2000). To date, no experimental data are available on the relative contributions of cholinergic inputs to the OB and PC on odor perception and learning.

The present work uses a computational model of the OB and PC and their common cholinergic inputs to investigate how bulbar cholinergic modulation affects cortical odor processing. We show that cholinergic modulation in the OB could increase contrast and synchronization in Mi cell output, leading to more effective learning of odor memories in the cortical network. Pyr cell networks trained with modulated inputs from the bulb exhibit more robust learning, recover memories from corrupted and/or lower-concentration stimuli better, and have higher storage capacity than those trained with unmodulated bulbar inputs. We conclude that cholinergic inputs to the OB and PC could act in concert to improve odor learning.

METHODS

Network Architecture

Our model is composed of two distinct networks representing the OB and the PC, each comprising principal cells and interneurons, as shown in Fig. 1*A*.

The OB model consists of four groups of cells: olfactory sensory neurons (OSNs), Mi cells, PG cells, and Gr cells. The axons of subsets of OSNs expressing the same olfactory receptor converge to one specific glomerulus inside the bulb (Mombaerts et al. 1996; Schoenfeld and Knott 2004), exciting dendrites of Mi cells and PG cells (Shepherd 1998). In our model, each OSN represents a large group of OSNs expressing the same odorant receptor. Therefore, the activity of these cells is not represented by discrete spikes but rather by a continuous output variable representing the average instantaneous firing probability of a large group of neurons expressing the same receptor (see *Eq. 3* for details). Each glomerulus is innervated by one Mi and one PG cell representing the average activities of cells associated with that glomerulus (Linster and Cleland 2002, 2004); therefore variations in the activity of different groups of Mi cells

Address for reprint requests and other correspondence: C. Linster, Dept. of Neurobiology and Behavior, Cornell Univ., Ithaca, NY 14853 (e-mail: cl243@cornell.edu).

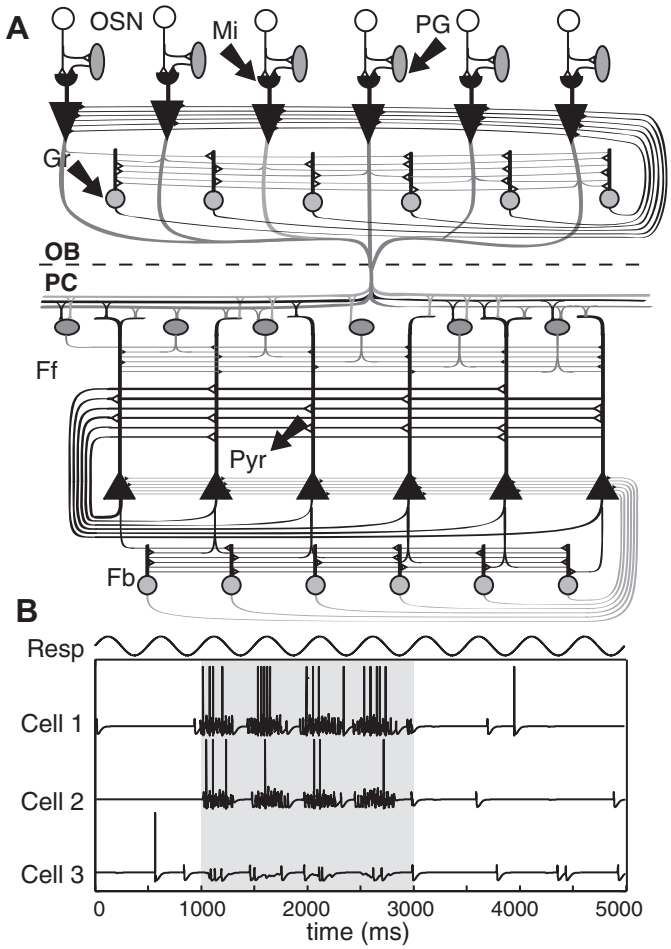

Fig. 1. *A*: simplified structure of the olfactory bulb (OB) and piriform cortex (PC). Olfactory sensory neurons (OSNs) expressing the same receptor converge to 1 specific glomerulus, where they connect with mitral (Mi) and periglomerular (PG) cells. Mi cells are the principal cells within the OB and project their axons to the PC, and they are modulated by 2 groups of interneurons: PG cells and granule (Gr) cells. Gr cells connect to Mi cells through dendrodendritic synapses: the Mi-Gr synapses are excitatory, and the Gr-Mi synapses are inhibitory. In the PC, Mi cells axons connect to pyramidal (Pyr) cells and a group of inhibitory interneurons called feedforward (Ff) cells that project their axons to the apical dendrites of Pyr cells, modulating the excitatory input coming from the OB (Stokes and Isaacson 2010). Pyr cells work as an autoassociative network, projecting their axons to other Pyr neurons and to a second group of inhibitory interneurons called feedback (Fb) cells (Marr 1971; Stokes and Isaacson 2010). Arrows indicate groups of cells modulated by ACh. *B*: Mi cell response to a single odor. The network was exposed to a specific odor for 2 s (gray region). *Cells 1*, *2*, and *3* show examples of Mi cells connected to glomeruli with different affinities to this odor. The neuronal activity on the network is modulated by the 2-Hz respiratory rhythm (Resp).

inside the same glomerulus (Dhawale et al. 2010) are not addressed here.

Mi cells are the principal neurons on the OB and transmit information to the PC. The information conveyed to Mi cells by OSNs is determined by both the odorant affinity of the OSNs projecting to them and their interactions with bulbar interneurons (see Fig. 1*A*). PG cells affect Mi cell activity locally within a glomerulus by directly inhibiting Mi cell primary dendrites (Linster and Cleland 2002, 2004). All PG synaptic inputs and outputs are localized on spine bodies located in their dendrites. These dendritic spines produce low-threshold bursts and release neurotransmitter independent of somatic action potentials (Cleland and Sethupathy 2006; McQuiston and Katz 2001); as a consequence these cells are nonspiking in the model.

Other interneuron interactions, such as short axon and external tufted cells, which have been previously modeled (Cleland et al. 2007), are not included in the present model. Mi cells also have dendrodendritic reciprocal connections between their secondary dendrites and dendrites of Gr cells. In these connections the contacts from Mi to Gr cells are excitatory and those from Gr to Mi cells are inhibitory (Shepherd 1998). In our model, each Mi cell is randomly connected to 40% of the Gr cells, similar to previous models (Linster et al. 2009). Mi cells are composed of two different compartments; as a result, the interactions with the two groups of interneurons (PG and Gr cells) are isolated from each other (more details below). For all simulations presented here, the OB model consisted of 50 OSNs, 50 PG cells, 50 Mi cells, and 50 Gr cells.

Mi cells project to the PC network, composed of Pyr cells and two types of interneurons: feedforward (Ff) and feedback (Fb) cells (Stokes and Isaacson 2010). The present network is composed of 50 Pyr cells, 50 Ff neurons, and 50 Fb neurons. For the connectivity between the OB and PC, we assume that each Pyr is randomly connected to 20% of Mi cells from the OB network, as determined previously (Linster et al. 2009). One important characteristic of this network is the presence of autoassociative fibers interconnecting Pyr cells; each Pyr cell is connected to 20% of the total Pyr network (Linster et al. 2009). The inclusion of feedback interactions between PC and OB would go beyond the scope of the present model, which focuses on how modulation of bulbar representations affects cortical processing.

In the PC, two interneuronal circuits modulate Pyr cell activity. The first group is composed of Ff neurons. In vivo recordings of odorant-evoked excitatory and inhibitory postsynaptic currents demonstrate that, across the cortical population, local Ff interneurons are activated by many different odorants, in contrast to Pyr neurons, whose activation is much more odorant specific. This first group of interneurons is connected to distal apical dendrites of Pyr cells (Isaacson 2010; Poo and Isaacson 2009; Stokes and Isaacson 2010). In our model, each Pyr neuron is inhibited by 30% of the Ff network, as measured by Stokes and Isaacson (2010). Ff cells, however, receive excitatory inputs from a larger number of Mi cells (40%; for details see RESULTS) than the Pyr cells (Poo and Isaacson 2009; Stokes and Isaacson 2010). Fb cells compose the second group of interneurons. They are recruited by excitation from Pyr neurons. Here we use connectivity similar to the findings of Stokes and Isaacson (2010), that is, each Fb cell is excited by 18% of the Pyr network and each Pyr cell is inhibited by 35% of the Fb network.

Neuron and Synapse Equations

All neurons are represented as single compartments, with the exception of Mi cells that are composed of two compartments. The evolution of the membrane voltage over time in each compartment is described by a first-order differential equation adopted from previous works (Linster and Cleland 2002; Linster et al. 2007, 2009):

$$\tau \frac{dv(t)}{dt} + v(t) = V^{ext}(t) \quad (1)$$

where τ is the membrane time constant, $V^{ext}(t)$ is the total external input over time, and different neurons receive different external inputs (Fig. 1*B* shows examples of Mi cells); for the complete list of parameters see Table 1. The input from a particular presynaptic neuron at time t is a function of the synaptic strength W_{ij}, the conductance change $g_i(t)$ in cell i, and the difference between the Nernst potential $E_{N,ij}$ of the specific channel type and the current membrane potential $v_j(t)$ of the postsynaptic neuron j, as described in *Eq. 2*:

$$V_j^{ext}(t) = W_{ij} g_{ij}(t)\left[E_{N,ij} - v_j(t)\right] \quad (2)$$

Table 1. *Model parameters*

General parameters (shared by all neurons)	$v^{hyper} = -10$ mV; $\theta^{min} = -2$ mV
Olfactory sensory neurons (OSN)	$\tau = 5$ ms; $\beta = 1$; $\theta^{max} = 15$ mV
Mitral cells (Mi, apical compartment)	$\tau = 5$ ms; $\beta = 1$; $\theta^{max} = 15$ mV/5 mV*
Mitral cells (Mi, soma compartment)	$t^{refrac} = 2$ ms; $\tau = 20$ ms; $\beta = 2$; $\theta^{max} = 15$ mV/5 mV*
Periglomerular cell (PG)	$\tau = 2$ ms; $\beta = 1$; $\theta^{max} = 9$ mV/4 mV*
Granule cell (Gr)	$t^{refrac} = 2$ ms; $\tau = 15$ ms; $\beta = 3$; $\theta^{max} = 13$ mV/8 mV*
Pyramidal cell (Pyr)	$t^{refrac} = 2$ ms; $\tau = 10$ ms; $\beta = 10$; $\theta^{max} = 17$ mV
Feedforward cell (Ff)	$t^{refrac} = 2$ ms; $\tau = 5$ ms; $\beta = 5$; $\theta^{max} = 17$ mV
Feedback cell (Fb)	$t^{refrac} = 2$ ms; $\tau = 5$ ms; $\beta = 5$; $\theta^{max} = 17$ mV
Afferent, OSN to PG	$g^{max} = 0.166$; $E_N = +70$ mV; $\tau_1 = 1$ ms; $\tau_2 = 2$ ms
Afferent, OSN to Mi (apical)	$g^{max} = 0.27$; $E_N = +70$ mV; $\tau_1 = 1$ ms; $\tau_2 = 2$ ms
Mi (apical) to Mi (soma)	$v^{max} = 1.5e^{-3}$†
Interglomerular inhib., PG to Mi (apical)	$g^{max} = 0.095$; $E_N = -10$ mV; $\tau_1 = 4$ ms; $\tau_2 = 8$ ms
Secondary dendrites, Mi to Gr	$g^{max} = 0.08$; $E_N = +70$ mV; $\tau_1 = 1$ ms; $\tau_2 = 2$ ms
Feedback inhibitory, Gr to Mi	$g^{max} = 0.475$; $E_N = -10$ mV; $\tau_1 = 4$ ms; $\tau_2 = 8$ ms
Mi to Pyr	$g^{max} = 0.84$; $E_N = +70$ mV; $\tau_1 = 1$ ms; $\tau_2 = 2$ ms
Mi to Ff	$g^{max} = 2.4$; $E_N = +70$ mV; $\tau_1 = 1$ ms; $\tau_2 = 2$ ms
Feedforward inhibition	$g^{max} = 0.056$; $E_N = -10$ mV; $\tau_1 = 4$ ms; $\tau_2 = 8$ ms
Feedback inhibition	$g^{max} = 0.8$; $E_N = -10$ mV; $\tau_1 = 4$ ms; $\tau_2 = 8$ ms
Pyr to Fb	$g^{max} = 0.8$; $E_N = +70$ mV; $\tau_1 = 1$ ms; $\tau_2 = 2$ ms
Pyr association fibers	$g^{max} = 7.2/5.0$‡ $E_N = +70$ mV; $\tau_1 = 1$ ms; $\tau_2 = 2$ ms

*Different weights are without/with cholinergic modulation, respectively. †The 2 Mi compartments are electrically coupled, and the output computed in the apical compartment is directly applied to the soma compartment (see METHODS for reasoning). ‡g^{max} in association fibers is slightly reduced for simulations in Figs. 8 and 9.

The communication between neurons in the network occurs either through discrete action potentials (for all the spiking neurons) or through continuous output, both a function of the membrane potential:

$$F_i(V) = \begin{cases} 0 & \text{if } V \le \theta^{min} \\ \left(\dfrac{V - \theta^{min}}{\theta^{max} - \theta^{min}}\right)^{\beta} & \text{if } \theta^{max} < V < \theta^{min} \\ 1 & \text{if V} \ge \theta^{max} \end{cases} \quad (3)$$

where $F_i(V)$ represents the continuous output (for OSNs and PGs) or the instantaneous spiking probability (for the remaining neuronal groups). θ^{min} and θ^{max} represent the minimum threshold and the saturation threshold of the output/probability function, respectively; β defines the nonlinearity of $F_i(V)$. For continuous presynaptic cells $g_i(t) = g^{max} \cdot F_i[\nu(t)]$; for spiking presynaptic cells $g_i(t) = g(t - t_i^{fire})$ with the time course of the conductance given by *Eq. 4*:

$$g(t) = g^{max}(e^{-t/\tau 1} - e^{-t/\tau 2}) \quad (4)$$

where τ_1 and τ_2 are, respectively, the rising and falling times of the conductance and g^{max} is a constant with no unit representing the maximum conductance of a given channel. After firing, the voltage of each spiking neuron is reset to a hyperpolarization potential v^{hyper} and remains inactive for a refractory period t^{refrac}.

Mi cells are composed of two distinct compartments: one representing their apical dendrite (apical compartment) and the other representing lateral dendrites and soma (soma compartment). Each of these compartments performs a separate cellular computation by interacting with different cell groups. The two compartments are electrically coupled, and the output computed in the apical compartment $F(V_{apical})$ is multiplied by the parameter v^{max} and directly summed to the membrane potential of the soma compartment. The soma compartment represents the integration site for all Mi cell input and generates action potentials.

The excitatory inputs to the bulb are modulated by a 2-Hz sinusoidal wave mimicking respiration frequency; the respiratory modulation does not influence the results that are based on simulations covering multiple respiratory cycles. All simulations were implemented with the MATLAB programming language, with a Euler integration method for the differential equations with a time step of 0.5 ms. The ModelDB accession number for the models reported in this paper is 146813 (Hines et al. 2004). The statistical significance of the results was evaluated with two-sample *t*-tests. For a summary of the parameters used in these simulations, see Table 1.

Plasticity

For the synaptic modifications of the pyramidal associative fibers we implemented a Hebbian learning similar to that proposed by Jensen et al. (1996). That is, the synaptic efficiency will be enhanced if both pre- and postsynaptic neurons fire together and reduced if not. Each Pyr-Pyr connection has a synaptic weight initially set to a random minimal value between 0 and 0.02, which is ~10% of the average maximum W observed after one training session in our network (see RESULTS for details). The synaptic enforcement has been shown to depend on NMDA receptors that allow the influx of Ca^{2+}, as long as sufficient postsynaptic depolarization is provided. The rise of Ca^{2+} triggers a cascade of events that ultimately results in a long-term potentiation (LTP) in AMPA- and NMDA-mediated synaptic responses (Bliss and Collingridge 1993). We assume that the postsynaptic depolarization is attributed to backpropagation from the action potential of the postsynaptic cell described by *Eq. 5*:

$$i^{post}(t) = \frac{t}{\tau^{post}} \exp\left(1 - \frac{t}{\tau^{post}}\right) \quad (5)$$

where the time course of this depolarization at the postsynaptic neuron (τ^{post}) is 2 ms.

The kinetics of NMDA channels depend on the binding of glutamate on the receptors. In the model, its time course is described by *Eq. 6*:

$$b^{glu}(t) = \exp\left(-\frac{t}{\tau^{NMDAf}}\right)\left(1 - \exp\left(\frac{t}{\tau^{NMDAr}}\right)\right) \quad (6)$$

where $\tau^{NMDAf} = 7$ ms and $\tau^{NMDAr} = 1$ ms characterize the kinetics of NMDA receptors. Finally, the synaptic enhancement between neurons i and j is described by *Eq. 7*:

$$\frac{dW_{ij}^{syn}}{dt} = (1 - W_{ij}^{syn}) \frac{i^{post}(t - t_j^{fire}) b^{glu}(t - t_j^{fire} - t^{delay})}{\tau^{pp}} + (0 - W_{ij}^{syn}) \left(\frac{i^{post}(t - t_i^{fire})}{\tau^{npp}} + \frac{b^{glu}(t - t_j^{fire} - t^{delay})}{\tau^{pnp}} \right) \quad (7)$$

where t^{delay} is the time it takes an action potential to travel from the soma to the synapses of a recurrent collateral. If i^{post} and b^{glu} peak together, the synaptic weight between neurons i and j is driven to one with the characteristic time τ^{pp} (50 ms); if the events are asynchronous, the synaptic efficacy is decreased with time τ^{pnp} ($\tau^{pnp} = \tau^{npp} =$ 250 ms).

Odor Stimulation

Each odorant is characterized by a distribution of affinities across the OSNs; these affinities are represented in our model by the activation of these OSNs elicited by a given odorant: the higher the activation, the higher the odor affinity. We generate 50 different affinity values that are randomly permutated to represent each odorant. This ensures that all odors impose the same average input to the OSN layer. The numerical values of the affinities are calculated from the normal probability density function $N(x,\mu,\sigma)$ for, $x = 1, 2, \ldots, 50$ (the total number of OSNs in our network), with $\mu = 25$ and $\sigma = 10$, and directly define OSN outputs. As a result, an odor stimulation is characterized by a distribution of OSN outputs ranging between 0 and max-concentration, with max-concentration = 1.0 unless otherwise noted. For all simulations reported in RESULTS, affinity values for each odorant are randomly distributed across the OSN population; however, in some figures these were centered at *neuron 25* and not randomly distributed for ease of visualization only.

Analysis

Sparseness. To evaluate the selectivity of the activation one odorant elicits in the population of neurons, we measure the level of sparseness in the neuronal response (Poo and Isaacson 2009; Rolls and Tovee 1995), defined by *Eq. 8*:

$$S = \frac{1 - \left(\left(\sum_{i=1}^{N} \frac{R_i}{N}\right)^2 \Big/ \sum_{i=1}^{N} \frac{(R_i)^2}{N}\right)}{1 - 1/N} \tag{8}$$

where R_i is the average firing rate of cell i when exposed to a given odor pattern and N is the total number of cells.

A response is highly sparse ($S = 1$) when a single cell is active, while it has minimal sparseness ($S = 0$) when all cells have the same activity.

Pairwise overlap between odor representations. To measure the similarity or difference between the representations evoked by a pair of distinct odors, we quantify how overlapped the network activities evoked by these odorants are. The odor representations in the OB and PC are composed of 50-element activity vectors where each element represents the average output activity (average number of spikes/s) of the corresponding Mi (for the bulb) or Pyr (for the cortex) cell over the course of a 7-s simulation. The similarity between two odor-evoked activities is calculated as the normalized dot product between the corresponding 50-element activity vectors O_1 and O_2 (Linster and Cleland 2010):

$$D_{O_1O_2} = \frac{\sum_{i=1}^{N} O_{1i}O_{2i}}{\|O_1\|\|O_2\|} \tag{9}$$

where O_{1i}, O_{2i} are the elements of the activity vectors O_1 and O_2, respectively, and $\|O_1\|$, $\|O_2\|$ are the norms of vectors O_1 and O_2.

Synchronization. A typical measure of synchrony between two neurons is the ratio of the spike cross-correlation using a small time bin τ and the mean spike activity between the two neurons [in Wang and Buzsaki 1996, the geometric mean is used, and the measure is called $\kappa_{ij}(\tau)$]. A problem with $\kappa_{ij}(\tau)$ and similar measures is the fact that it increases with neural activity even when neurons fire random uncorrelated spikes (Wang and Buzsaki 1996). A convenient measure should remove this confound. We therefore define the level of coherence between two neurons as

$$c_{ij} = \left[1 - \frac{\sum_{l=1}^{K} X_{i'}(l)X_{j'}(l)}{\sum_{l=1}^{K} X_i(l)X_j(l)}\right]_+ \tag{10}$$

where $[x]_+ = \max(0,x)$ indicates linear rectification. The cross-correlation between neurons i and j is compared to the cross-correlation that would be observed in random spiking neurons i' and j', with the same firing rates of neurons i and j. $X_i(l) = 0$ or 1 indicates the event of a spike in neuron i in the time bin $[(l-1)\tau, l\tau]$ where $l = 1, 2, 3, \ldots, K$, $\tau = T/K = 2$ ms (that is, 2 spikes are considered synchronized if they occur within 2 ms apart), and T is a long time interval. The numerator in *Eq. 10* can be approximated by $n_i n_j/K$, where n is the number of spikes of a neuron in the interval T. The population coherence measure c is defined by the average of c_{ij} over many pairs of neurons in the network. With this method, c is bounded between 0 and 1: 0 when the network shows absolutely no spiking coherence (or there is anticorrelation) and progressively higher as the neurons synchronize.

Simplified model of PC inputs. An abstract model of Mi cell firing was implemented to explore how Mi coherence and sparseness independently influence cortical processing. This abstract model allows us to change sparseness and coherence independently of each other, which is not possible in the OB model because of reciprocal dependence between these effects. In this abstract model, the firing rate of a Mi cell i at time t is defined by

$$p_i(t) = A_i r \frac{\left[1 - \cos(2\pi f t)\right]^{\delta}}{\frac{1}{T}\int_0^T \left[1 - \cos(2\pi f t)\right]^{\delta} \mathrm{d}t} \tag{11}$$

where $0 < A_i \leq 1$ is the affinity of neuron i to a given odorant (see Fig. 2 for details), r sets the average firing rate in response to the odor stimulation, T is the modulation period (in ms), $f = 1/T$ is the frequency of modulation, and δ controls the duration of the positive excursion of the oscillation. Observe that δ does not change the firing rate. After each spike, p is clamped to 0 for 30 ms to avoid bursts during the firing cycles. This short period of inactivity was adopted to better fit the simulation using the integrate and fire model and should not be interpreted as a direct equivalent of the refractory period in Mi cells. The distribution of A_i in response to an odorant controls sparseness in the network (Fig. 2*A*), whereas the parameter δ controls how tightly together Mi cells fire (synchronization; Fig. 2*B*).

Strength of PC response. The response strength of the Pyr network to a particular odorant is measured in two ways: *1*) the average firing rate of all cells in the network in response to the odorant and *2*) the average firing rate of the cells considered to be responsive to the odorant. To be classified as "responsive" the average firing rate of a given neuron during a 7-s odor presentation must exceed the mean network activity rate by two standard deviations.

Cholinergic Modulation

Experimental data show that cholinergic modulation changes cellular and synaptic properties of the OB and PC networks. In the OB, it increases the excitability of PG and Mi cells through nicotinic receptors (Castillo et al. 1999; Chaudhury et al. 2009; Ravel et al. 1990), increases afterdepolarization, and decreases afterhyperpolarization responses in Gr cells through muscarinic receptors (Nickell and Shipley 1988; Pressler et al. 2007). Cholinergic modulation in these three cell groups was implemented by decreasing the saturation threshold (θ^{max} in *Eq. 3*), which effectively increases the excitability of the cells. In isolated cells, Mi cell firing increased by 3.1-fold with the parameters chosen here, approximately matching an experimen-

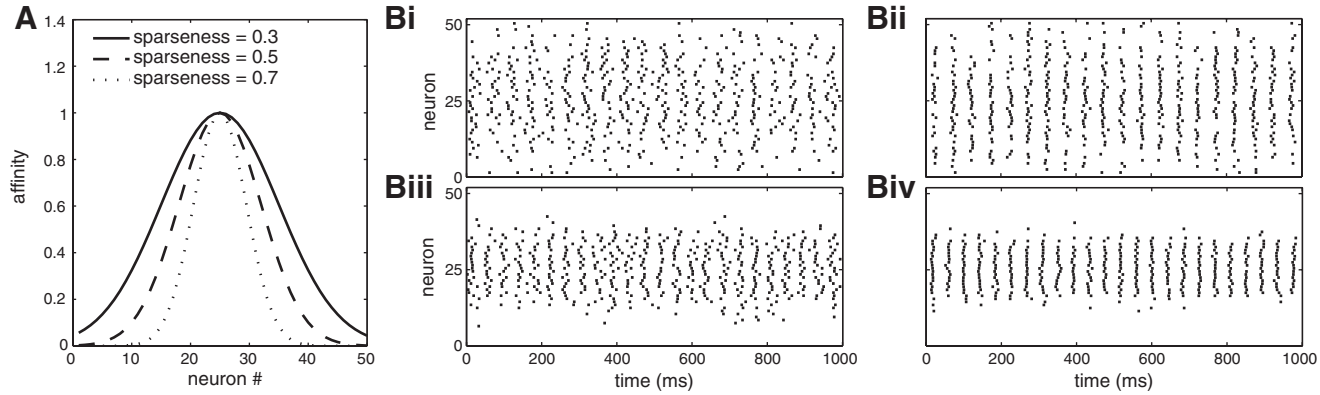

Fig. 2. Abstract model for Mi cell activity. To test the roles of sparseness and coherence in Pyr cell codification, we created a simplified model of Mi cell output, where these features (as well as Mi cell frequency) can be independently altered. *A*: odor affinity implementation in this model is similar to the OSN affinity distribution (OSN activation distribution). These affinities are calculated from the normal probability density function $N(x,\mu,\sigma)$ for, $x = 1, 2, \ldots, 50$ (the total number of OSNs in our network), with $\mu = 25$, and randomly distributed across the neurons. For ease of visualization, we show here a distribution centered on *neuron 25* and not randomly distributed. The value of σ determines the level of sparseness in our network. The graph shows examples of weak (solid line), medium (dashed line), and strong (dotted line) sparseness. *B*: sparseness, coherence, and frequency can be independently modified. The graphs show examples of Mi output with different levels of sparseness and coherence. *Bi*: low sparseness (0.22) and coherence (0.3). In this example the parameters adopted are $r = 26$, $f = 18$, $\delta = 0.95$, and σ (from normal probability density function) = 10.2. *Bii*: low sparseness (0.21) and high coherence (0.7), where $r = 26$, $f = 18$, $\delta = 6.5$, and $\sigma = 10.2$. *Biii*: high sparseness (0.59) and low coherence (0.32), where $r = 60$, $f = 18$, $\delta = 0.8$, and $\sigma = 5$. *Biv*: both high sparseness (0.58) and coherence (0.7). For this, we use $r = 90$, $f = 22$, $\delta = 6.9$, and $\sigma = 4.7$. In all these raster plots, the average frequency was kept at ~8 Hz.

tally reported 3.7-fold increase (Castillo et al. 1999). Firing in Gr cells increased by 2.3-fold, close to the experimentally reported 2.6-fold (Pressler et al. 2007). The increase we implemented in PG cells was higher than that reported experimentally (60% vs. 45% in Ravel et al. 1990); however, we measured this increase in isolated cells, whereas the data reported by Ravel et al. (1990) were obtained in vivo. PG cell modulation was additionally constrained by the need to keep average Mi cell firing constant, as detailed below.

Cholinergic modulation increases both inhibition and excitation onto OB mitral cells; as a consequence, the balance of excitation and inhibition can be kept constant with ACh ON or OFF. In our simulations, the average Mi output frequency was not significantly affected by ACh (see Fig. 5*A*). This balancing helps to ensure that the effects on cortical learning observed are a result of the changes in sparseness and coherence and not due to changes in Mi average spiking activity. The balancing of inhibition and excitation corresponds to experimental results in which no change in Mi spontaneous or odor-evoked activity was found when cholinergic modulation was increased or decreased (Chaudhury et al. 2009). Here we only simulate cholinergic inputs from the HDB; therefore, cholinergic receptors on sensory neurons, as described experimentally (Li and Matsunami 2011), are not included. A summary of the parameters adopted in the simulations can be found in Table 1.

In the PC, ACh suppresses excitatory synaptic transmission between Pyr cells while promoting LTP between these synapses (Hasselmo and Barkai 1995; Hasselmo and Bower 1992; Williams and Constanti 1988). For simplicity, we assume that ACh switches the dynamics of the Pyr network between learning (ACh ON) and recalling (ACh OFF) modes, as proposed by Liljenstrom and Hasselmo (1995): when cholinergic modulation is ON in the model (learning mode), Pyr-Pyr synaptic transmission is reduced to 40% of its original value (Hasselmo and Bower 1992; Hasselmo and Cekic 1996) and the synaptic plasticity mechanisms (*Eqs. 5*, *6*, and *7*) are active. When cholinergic modulation is absent (recall mode), Pyr-Pyr connections are fully functional and synaptic plasticity is inactive.

RESULTS

Olfactory Bulb to Piriform Cortex Connectivity

The connectivity between OB and PC is poorly understood. According to current understanding, Mi axons project to a large number of Pyr neurons with no clear pattern, which makes the use of any anatomical or functional activity map extremely limited (Buonviso et al. 1991; Nagayama et al. 2010; Ojima et al. 1984). As a consequence, we assume a previously used strategy of randomly connecting Mi and Pyr cells (see METHODS for details; Linster et al. 2007, 2009). The network parameters, specifically the number of projections from the OB to PC, their synaptic weights, and the thresholds of PC neurons were then adjusted to best replicate the available experimental data (Poo and Isaacson 2009). Recent experimental evidence (Davison and Ehlers 2011) indicates that Pyr cells respond not to single-glomerulus input but to inputs from specific glomerular ensembles. To reproduce these data, synaptic weights and firing thresholds were adjusted such that any given Pyr cell fires in response to synchronized input from approximately four Mi cells (Davison and Ehlers 2011), as shown in Fig. 3*A*. To adjust the parameters, the PC network was simulated 150 times with different, randomly chosen odor patterns, and the weights and thresholds were adjusted so that every time a Pyr cell fired there were at least four presynaptic Mi cell spikes within the 15-ms integration time, as shown in Fig. 3*B*.

Roles of PG and Gr Cell Modulation in Mi Cell Odor Responses

Previous works suggested distinct roles for PG and Gr networks for bulbar odor representations: PG-Mi interactions would be involved in contrast enhancement (Cleland and Sethupathy 2006; Mandairon et al. 2006), and the Gr-Mi interactions would promote Mi synchronization (Lagier et al. 2004; Li and Hopfield 1989; White and Kauer 2001). Before investigating the effects of ACh modulation in the complete OB model, we investigated the modulation of each type of interneuron individually. We first studied PG-Mi interactions while turning the Gr-Mi connections off; second, we tested the Gr-Mi interaction while turning off the PG-Mi connections.

ACh does not modulate OSN responses in our model (Fig. 4*Ai*); therefore any changes in Mi cell responses are due to changes

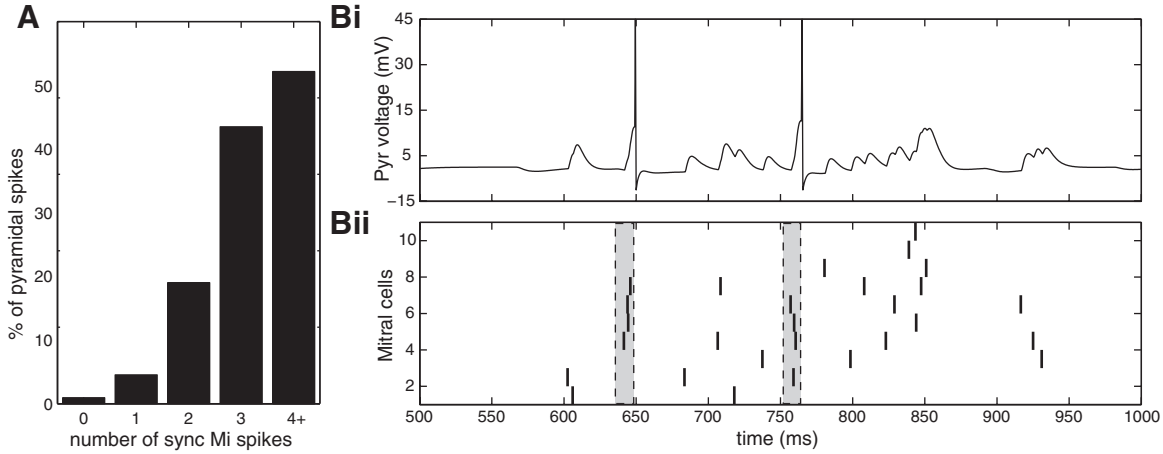

Fig. 3. Pyr cell firing depends on synchronized input. *A*: no. of Pyr cell spikes evoked by 0–4 synchronous presynaptic spikes (using a 15-ms integration time). The Mi-Pyr connection strength was set such that the majority of pyramidal spikes were elicited by synchronized firing of at least 4 Mi cells (Davison and Ehlers 2011). *B*: changes in the membrane potential of 1 Pyr cell (*Bi*) and a raster plot of all Mi cells connected to that cortical neuron (*Bii*). Gray area in *Bii* indicates 15-ms time window before each Pyr action potential.

in internal OB processing. In this and the other graphs in Fig. 4, responses to a single odorant are illustrating the modulation effects; for ease of visualization only, odor response distributions are centered on *glomerulus 25* and not randomly distributed. Increasing PG cells' excitability in response to ACh modulation reduces sparseness in PG cells because they respond to a broader range of odorants (Fig. 4*Aii*). Mi and PG cells from the same glomerulus have the same OSN inputs but different response properties (see Fig. 2*C* in Cleland and Linster 2005). Mi cell activity is directly influenced by PG-mediated dendrodendritic inhibition, such that only the most strongly excited Mi cells are activated, a process known as nontopographical contrast enhancement based on local glomerular computations (Cleland and Sethupathy 2006). In Fig. 4*Aiii*, we show the effect of PG modulation on Mi cell odor responses in three different scenarios: cholinergic modulation OFF in both PG and Mi cells, ACh ON only in PG cells, and ACh ON for PG and Mi cells. These different configurations are also displayed in Fig. 4*Aiv* as a raster plot (*top*) and a spike count (*bottom*), following the same order in Fig. 4*Ai* to help visualization. When ACh is OFF in both PG and Mi cells (from 0 to 2,000 ms), we observe a broad activation of the Mi network, indicating a low level of sparseness. In fact, the average sparseness over 50 different simulation tests is $S \approx 0.3$, similar to that conveyed to Mi cells by OSN (OSN sparseness also ~0.3). With PG modulation turned ON, local inhibition on Mi cells is stronger, the number of active Mi cells is reduced, and the average sparseness increases from ~0.3 to ~0.51 ($P < 0.001$). When cholinergic modulation in the apical compartment of the Mi cell is also turned ON, the overall activation of Mi cells increases, accompanied by a slight decrease in the average sparseness from ~0.51 to ~0.48 ($P < 0.001$). In these simulations, the average coherence stayed relatively constant around ~0.05.

Next, we investigated the influence of the Gr-Mi connections on Mi cell responses. As described before, Gr and Mi cells are connected through dendrodendritic synapses, where the Mi-Gr connections are excitatory and the Gr-Mi connections are inhibitory. This type of reciprocal interactions between excitatory principal cells and inhibitory interneurons was previously shown to create network synchronizations in artificial neural networks (Wang and Buzsaki 1996) as well as Mi synchronization in electrophysiology experiments (Lagier et al. 2004). When principal cells fire, they excite a group of interneurons, which in turn inhibits the principal cells in a process called feedback inhibition. As the inhibition in the principal cells wanes, these neurons are able to fire again. This process is repeated indefinitely, thereby generating an oscillation during which neurons synchronize. Figure 4*B* shows that a similar process is elicited between Mi and Gr cells in the OB model. We initially (first 2,000 ms) run the network with ACh modulation off for both Mi and Gr cells. The excitability of both cell groups is low, and Mi cell firing is too weak to drive the activation of Gr cells; therefore, the average coherence for both Mi and Gr cells is relatively low (C_{Mi} ~0.33 C_{Gr} ~0.54). Mitral sparseness is also low (S ~39). From 2,000 to 4,000 ms the cholinergic modulation in Gr cells is turned ON, increasing the excitability of these cells, resulting in an increase in the number of Gr cells responding to Mi cell inputs. Consequently there is an increase of feedback inhibition onto Mi cells, which leads to an increase in synchronization in Mi cells from ~0.33 to ~0.54 ($P < 0.001$) and in Gr cells from ~0.54 to ~0.63 ($P < 0.001$). We observe a slight increase in Mi sparseness from ~0.39 to ~0.43 ($P < 0.001$) when Gr cells receive cholinergic inputs. When ACh is ON in Mi and Gr cells, Mi cells' increased excitability potentiates the interplay between Mi and Gr cells, leading to an increase of the level of synchronization from ~0.54 to ~0.76 ($P < 0.001$) in Mi cells and from ~0.63 to ~0.78 ($P < 0.001$) in Gr cells. As the Mi cells become more excitable, the noise increases and the average sparseness drops from ~0.43 to ~0.36 ($P < 0.001$).

In summary, our results suggest that the PG-Mi connection affects the sharpness of an odor representation in Mi cells while the Gr-Mi connection mostly influences its synchronization.

Overall Effect of Cholinergic Modulation in OB: Increase in Mi Cell Sparseness and Coherence

To test the effect of ACh on odor representations in the OB, we measured the average sparseness and synchronization of Mi output when exposed to different odor patterns. As described in

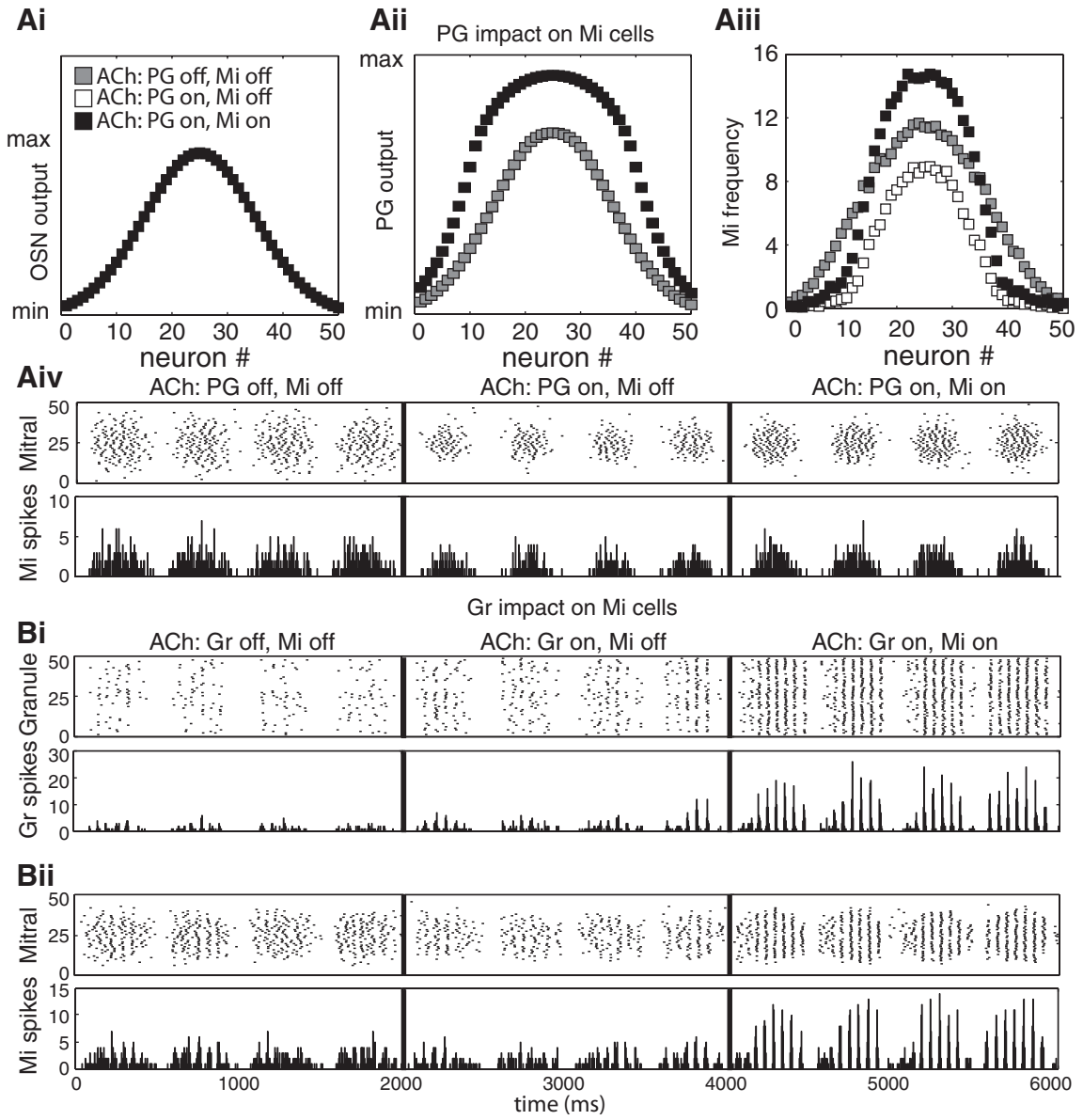

Fig. 4. Roles of PG and Gr cells in Mi activation. For easier visualization, odor affinities were set as a normal distribution centered on *neuron 25* to create these graphs. *A*: PG cells affect the sparseness of Mi cell output but show no impact on Mi synchronization. Connections between Mi and Gr cells were removed for these tests. *Ai*: distribution of OSN affinities to the odorant used to illustrate these effects. *Aii*: ACh modulation increases PG cell excitability, reducing sparseness in PG cells. Graph shows PG activation when ACh is OFF (gray) or ON (black). *Aiii*: ACh also increases the excitability of Mi cells, in addition to the increase in PG-mediated dendrodendritic inhibition. As PG excitability increases, this inhibition also becomes stronger, allowing only the most strongly excited Mi cells to fire. The overall effect is a decrease in the number of responsive cells (ACh: PG on, Mi off), accompanied by an increase in activity in responsive cells (ACh: PG on, Mi on). *Aiv*, *top*: raster plot of a Mi network in different cholinergic modulations. Initially, ACh is off for PG and Mi cells and the sparseness is low (S ~0.3). After 2,000 ms, PG modulation is turned ON, inhibition on Mi cells becomes stronger, and the sparseness increases to ~0.51. Finally, at 4,000 ms Mi modulation is also initiated, which increases Mi overall activation and slightly decreases sparseness to ~0.48. *Bottom*: spike count for the same simulations. *B*: Gr cells affect the synchronization of Mi cell outputs with some accompanying effects on Mi sparseness. Connections between Mi and PG cells were removed for these tests. *Bi* and *Bii*: during the first 2,000 ms, ACh modulation in both Mi and Gr cells is OFF, Gr excitability is weak, and the levels of Mi coherence and sparseness are low (C_{Mi} ~0.33, S ~0.39). The level of coherence in the Gr network is also relatively low (C_{Gr} ~0.54). After 2,000 ms, cholinergic modulation in Gr is turned ON, increasing the excitability of Gr cells, resulting in an increase in the number of active Gr cells and, in consequence, an increase of the feedback inhibition in Mi cells, which leads to an increase in synchronization for both Mi (C_{Mi} ~0.54) and Gr (C_{Gr} ~0.63) (see text for reasoning). Gr cells also play a role in Mi cell sparseness; we observe a slightly increased S ~0.43. As we turn ACh ON in both Mi and Gr cells the level of synchronization increases again (C_{Mi} ~0.76, C_{Gr} ~0.78), but the sparseness drops to ~0.36 as Mi become more excitable. The odor is applied during the total extent of each simulation. Results presented in *Aiii* are the average over 50 simulations.

METHODS, the average Mi network frequency in all OB simulations was kept around 4 Hz, independently of ACh modulation (Fig. 5*Ai*).

When ACh modulation is OFF, the Mi activation is broader, with more cells firing; the number of active cells is reduced when modulation is ON, with an accompanying increase in the frequency of well-tuned neurons (Fig. 5*Aii* shows an example of a response to a specific odor). Figure 5*Bi* shows that ACh modulation in the OB network results in a significant increase in mitral cell sparseness (from 0.42 to 0.58).

The increase in activation sparseness observed when ACh is ON also leads to a higher contrast between different odorants. We calculated the dot product (*Eq. 9*) as a measure of similarity between the Mi activation evoked by two different odorants when ACh is OFF or ON for different levels of similarity between OSN inputs (Fig. 5*Bii*). As the similarity between OSN inputs decreases, the similarity between Mi outputs also reduces, but this reduction is more pronounced when ACh modulation is ON. That is, ACh modulation decorrelates odor representations, in accordance with behavioral observations (Mandairon et al. 2006).

Synchronization among bulbar cells also increases under ACh modulation. Figure 5*Ci* shows that the level of synchronization increased from ~0.19 in the unmodulated condition (ACh OFF) to ~0.68 in the modulated condition (ACh ON). This is also evident when comparing the effects of ACh modulation in Fig. 5, *Di* and *Dii*. Similar to the results shown in Fig. 4*B*, ACh modulation increases the excitability of both Mi and Gr cells, which leads to an increase in the number of active Gr cells (the average network frequency increases from ~1.1 to ~4.2 Hz) and, consequently, an increase in the feedback inhibition onto Mi cells. The inhibition is now strong enough to synchronize Mi and Gr cells (Fig. 5, *Ci* and *Cii*). In summary, ACh modulation increases the sparseness and coherence of OB output to the PC.

Summary of Role of ACh Modulation in Different Neuronal Groups

In this section we summarize how Mi outputs change when the modulation is partial in select groups of neurons only. Because pharmacology experiments often use selective antagonists and agonists, it is important to know the effects of each modulation type individually: PG and Mi cells are modulated via nicotinic and Gr cells via muscarinic receptors.

Figure 6 summarizes how different configurations of modulation shape Mi cell output. For each of these configurations we turned ACh ON or OFF in one or more neuronal groups and measured Mi cells' coherence and sparseness; for each configuration 30 simulations were performed. At the opposite corners of the graph (Fig. 6, *bottom left* and *top right*), we observe the configurations previously explored when cholinergic modulation was OFF (○) or ON (□) in all neuronal groups. One can note that a state of high coherence and high sparseness can only be obtained when ACh is ON in Mi, PG, and Gr cells at the same time. It is possible to obtain an even higher coherence in Mi output when ACh modulation is blocked in PG cells but not in Mi and Gr cells (☆), which would be somewhat expected, given the results from Fig. 4*B*. Compared with the fully modulated network (□) the average coherence increases from ~0.68 to ~0.73 ($P < 0.001$), but this increase comes at the expense of a sparseness decrease from ~0.58 to ~0.47 ($P < 0.001$). On the other hand, we observe a very high sparseness in Mi output when ACh modulation is ON in PG and Gr cells, but OFF in Mi cells (~0.61, ▽). This configuration, however, also results in low synchronized Mi firing (~0.27).

The different configurations in the graph in Fig. 6 also help us to confirm the roles played by different neuronal groups in the Mi odor responses and independently investigated in Fig. 4. For instance, the cases resulting in the top four values of the sparseness measures (▲, ▽, ×, and □) share the fact that cholinergic modulation is ON in the PG cells; these results are also in accordance with the idea that nicotinic modulation of PG cells is the main factor responsible for contrast enhancement modulation (Cleland 2010; Cleland and Sethupathy 2006).

The effects on Mi synchronization seem to be more nuanced in our model network and, in some configurations, almost counterintuitive. Previous theoretical and experimental works linked Gr cells to Mi cell synchronization (Erdi et al. 1993; Grobler and Erdi 1991; Lagier et al. 2004; Li and Hopfield 1989; White and Kauer 2001), and simulations in Fig. 4*B* show similar effects. ACh ON in Gr cells always led to an increase in Mi coherence when the other modulations were kept constant (compare ▲ to ▽, ○ to *, ◇ to ☆, and × to □ in Fig. 6). However, the level of synchronization does not vary monotonically with ACh because of the nonlinearities of the feedback loop: although ACh modulation raises the level of synchronization by increasing Gr excitability, it leads to increased inhibition in mitral cells, resulting in less synchronization (Wang and Buzsaki 1996).

From an experimental perspective, the configurations represented by * and × in Fig. 6 are particularly interesting, for they, respectively, represent Mi sharpness and synchronization when nicotinic or muscarinic receptors are blocked in the OB. In our model, blocking muscarinic receptors in Gr cells (×) has a smaller effect on Mi cell sparseness than blocking nicotinic receptors (*), in accordance with similar observations with behavioral pharmacology by Mandairon et al. (2006), where the authors report smaller impairment in odor discrimination when blocking muscarinic receptors than in experiments where nicotinic receptors were blocked.

ACh Modulation in the Bulb Increases Selectivity and Response Amplitude of Cortical Pyramidal Cells

The simulations of the OB showed that ACh modulation increases synchronization (Fig. 5*Ci*) and sparseness (Fig. 5*Bi*) of Mi cell activity in response to odors. Our next step was to test how bulbar modulation affects PC responses to odorants. Figure 7*A* shows that cholinergic modulation in the OB significantly increases sparseness of Pyr cells to odorants from ~0.46 to ~0.62 ($P < 0.001$). In addition to the increase in sparseness, Pyr cell spiking frequency in response to odor inputs increases from ~0.44 to ~0.97 Hz ($P < 0.001$; Fig. 7, *Bi* and *Bii*). More specifically, the spiking frequency of odor-responsive Pyr cells increased from ~1.3 to ~ 4.9 Hz (Fig. 7*Bii*; see METHODS for details on the criteria for "responsive cells"), although the average frequency of Mi cell output was constant (around 4.0 Hz for both scenarios: ACh OFF and ON). This increase of spiking frequency is also evident in Fig. 7*C*, which shows raster plots of Pyr cell responses to one specific odorant. Pyr cell responses to odorants are increased when OB activity is modulated because of the Pyr cell dependence on synchronized Mi cell firing (Fig. 3, *A* and *B*), which is much more pronounced in the modulated state (as shown in Fig. 5, *Ci* and *D*).

Input Sparseness Directly Impacts Pyr Cell Sparseness and Memory Capacity, While Input Coherence Influences Pyr Response Amplitude and Learning Rate

So far, we had tested the PC network with bulbar modulation either OFF or ON. As a result, bulbar inputs would either show

high sparseness and high coherence or low sparseness and low coherence. Figure 6 shows that the interactions between Mi cells and the OB interneurons are very complex; for instance, we cannot ensure an increase in coherence that does not impact Mi sparseness and average frequency. To systematically investigate the effects of sparseness and coherence on cortical processing, we implemented a simplified Mi cell response model, in which sparseness, coherence, and frequency of the Mi input can be independently manipulated (see *Eq. 11* in METHODS).

Figure 8*A* shows the impact of different levels of input sparseness and coherence on Pyr sparseness, average frequency, and the frequency of active cells before learning. In these figures the *x*- and *y*-axes represent, respectively, the variation in coherence and sparseness of the Mi inputs to the PC; changes in each of the Pyr features are represented by a

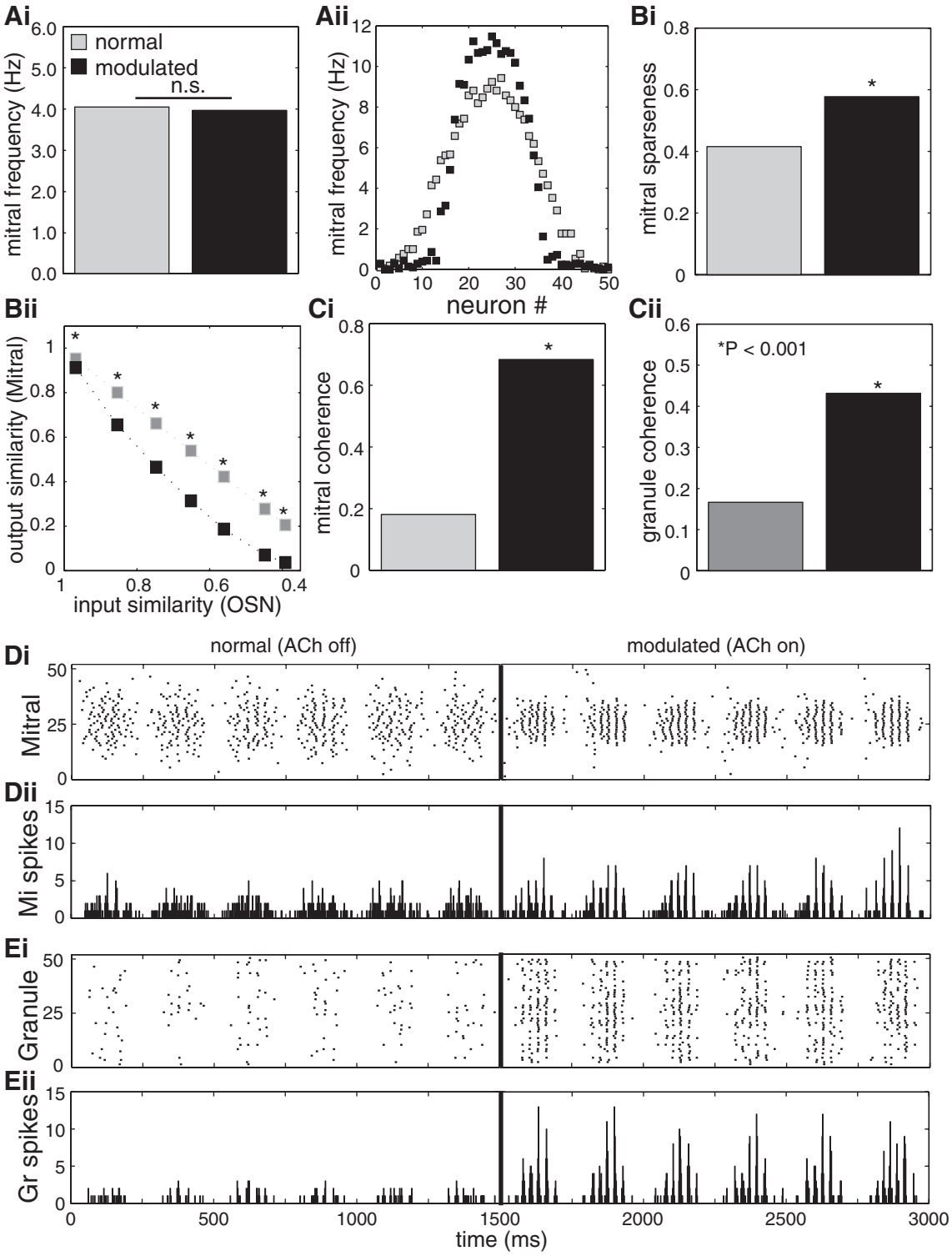

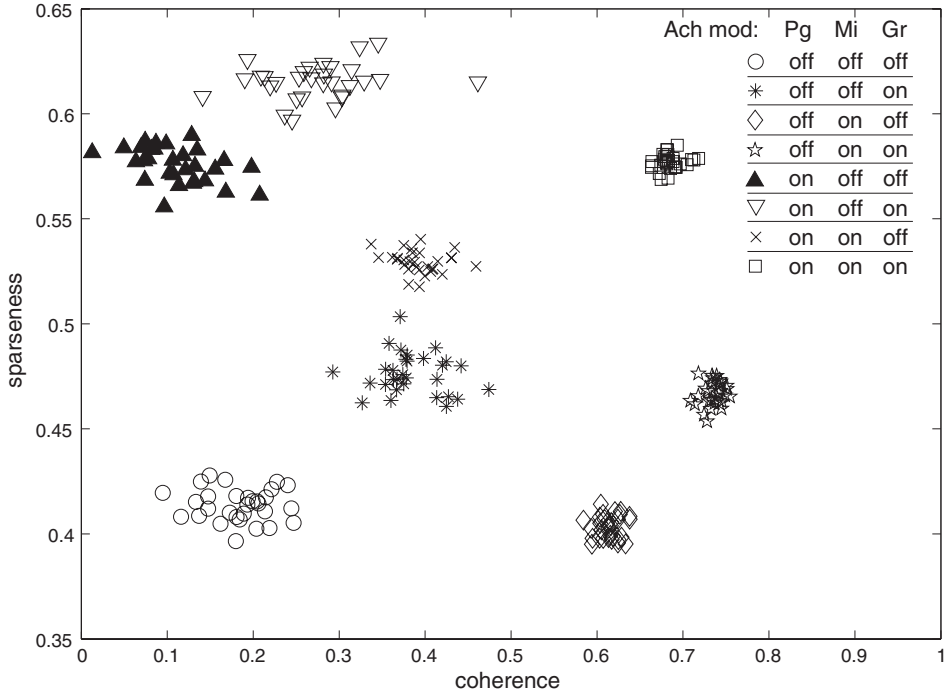

Fig. 6. Modulation of subpopulations of neurons: Mi cell sparseness and coherence as a function of the presence or absence of ACh in a particular set of cells. In each of these configurations, cholinergic modulation was turned ON or OFF in 1 or more neuronal groups and coherence and sparseness of odor responses in Mi cells were measured. Each configuration was run 30 times with random odors. Mi sparseness depends strongly on ACh modulation of PG cells, while coherence needs high activity in both Mi and Gr cells (see text for reasoning). At the opposite corners of the graph are the tests where cholinergic modulation was OFF (○) or ON (□) in all neuronal groups. Average Mi frequency for each configuration: ○ = 4.0 Hz; * = 2.9 Hz; ◇ = 7.1 Hz; ☆ = 5.9 Hz; ▲ = 2.6 Hz; ▽ = 2.0 Hz; × = 5.4 Hz; □ = 4.0 Hz.

grayscale code (lighter = high, darker = low). Figure 8*Ai* shows that Pyr sparseness is directly dependent on Mi sparseness, while the level of input coherence plays a minor role. The opposite is true for the average frequency (Fig. 8*Aii*): changes in the input synchronization impact Pyr cell activity; the effects of sparseness on Pyr activity, however, are less pronounced. Finally, Fig. 8*Aiii* shows that when only active cells are taken into consideration, both sparseness and synchronization are important. The signal-to-noise ratio ($F_{act\_cells}/F_{all\_cells}$) in response to inputs with high sparseness and high coherence is 4.5 but drops to 3.1 if we only increase coherence and leave the input sparseness low.

We then tested how input characteristics affect cortical learning (Fig. 8*B*). We trained the network with varying levels of sparseness and coherence and tested recall; during recall, input patterns were presented with low sparseness and coherence levels. This ensured that any effects we measured had a common baseline and were due to differences in training, not drive of cortical networks. Memories were trained for 4 s. Figure 8*Bi* shows that the sparseness of recalled memories depended on both high input sparseness and coherence during learning. Figure 8*Bii* shows that the Pyr activation during recall (after learning) is directly influenced by the level of input coherence during learning. Figure 8*Biii* shows that the frequency of cells considered active during recall depends entirely on the level of input coherence during learning. However, signal-to-noise ratio is higher in cases for which both input sparseness and coherence during learning were high: a signal-to-noise ratio of ~3.6 drops to 2.8 when sparseness is low (Fig. 8*Biii*, *bottom right* examples). The examples here show that Mi synchronization is crucial to improve learning and Pyr activation while the input sparseness increases the signal-to-noise ratio in the system.

Input sparseness impacts the number of memories that can be successfully stored in an autoassociative network (de Almeida et al. 2007; Treves and Rolls 1991). We trained two Pyr networks with sequences of the same odor inputs. In the first group each odor input had low sparseness ($S = 0.4$), while in the second group the sparseness was higher ($S = 0.6$). All other parameters were kept fixed (average input frequency ~8.0Hz; input coherence ~0.7). To test for memory capacity, we attempted to recall all memories previously trained in the network after each new insertion. The input memories during recall are versions of the orig-

Fig. 5. Cholinergic modulation increases sparseness and synchronization (coherence) of odor representation in principal cells of the OB. *A*: average Mi network frequency is kept fairly constant with or without ACh modulation. *Ai*: differences in frequency are not significant (n.s.) whether ACh is OFF (gray) or OFF (black). In both cases the average frequency is ~4.0 Hz. *Aii*: average frequencies are similar because there is a smaller group of cells firing at higher frequency when cholinergic modulation is ON (compare neuron frequencies in gray and black). One odor example with OSN affinities centered on *glomerulus 25* is shown. *B*: ACh modulation increases the sparseness of Mi cell odor responses and the contrast between different odorant inputs. *Bi*: sparseness of Mi outputs calculated with *Eq. 8*. The average Mi cell sparseness increases from ~0.41 when ACh modulation is OFF (gray) to ~0.57 when ACh is ON (black). *Bii*: the increase in the sparseness also leads to a higher contrast between odorants. The graph shows the similarity (calculated with the dot product from *Eq. 9*) of 2 Mi outputs in response to 2 different odorants (*y*-axis) as a function of the similarity between the corresponding OSN inputs (*x*-axis). As the similarity between OSN inputs decreases, the similarity between Mi outputs also decreases, but this reduction is more pronounced when ACh modulation is ON. *Ci* and *Cii*: ACh modulation increases the excitability of Mi and Gr cells, which results in increased synchronization of both cells (see Fig. 4*B* and text for reasoning). *D*: combined effect of PG and Gr cells on Mi activation. *Di*: raster plot of Mi cells when ACh modulation in the system is OFF and ON. One can observe an increase in the synchronization and noise reduction in the modulated state of Mi cells and an increase of synchronization in Gr cells. *Dii*: the increase of coherence is also evident if we count the number of synchronized spikes in 4-ms time bins. To help visualization, the odor affinities were set as a normal distribution centered on *neuron 25* (note that this does not correspond to the random distributions of affinities used in the simulations and detailed in METHODS). The odor is applied during the total extent of each simulation. Results presented in *B* and *C* are averages over 150 simulations.

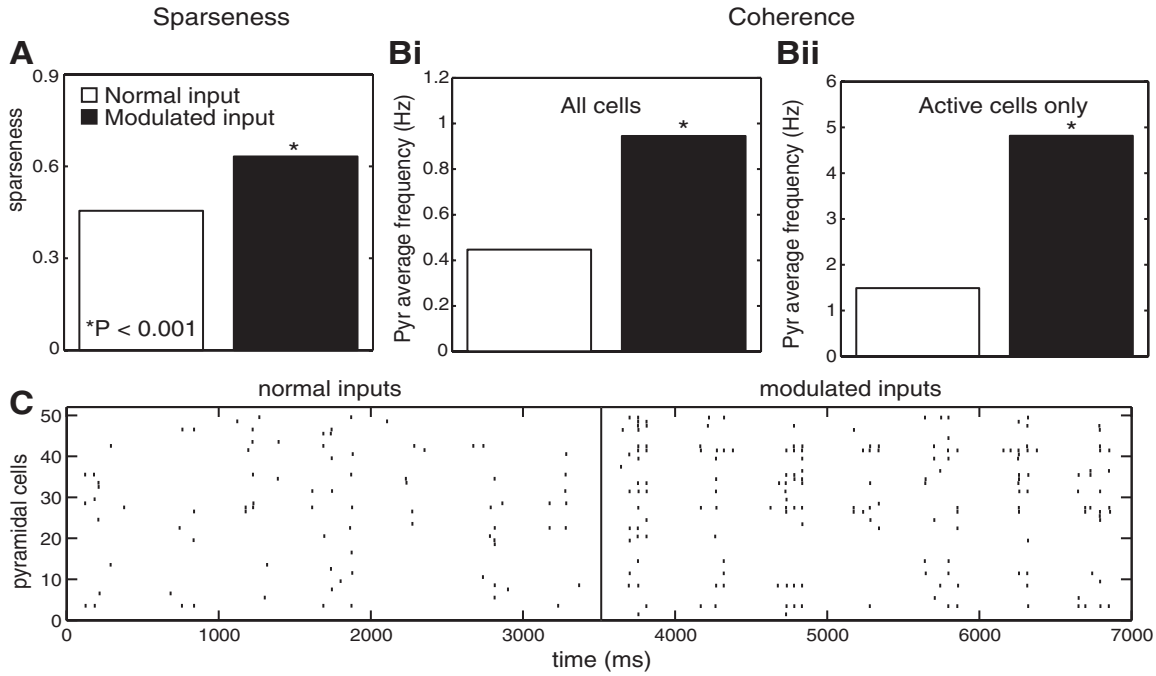

Fig. 7. Effect of cholinergic modulation in the OB on cortical odor responses. *A*: sparseness of Pyr cell odor responses. Cholinergic modulation in the OB significantly increases the sparseness of Pyr cell activity in the PC. Graph shows average sparseness of odor representation in Pyr cells when Mi input was unmodulated (normal) or modulated by ACh. *Bi*: cholinergic modulation also increases the average frequency of the Pyr cell network. In this graph, the open bar represents the average firing rate of all Pyr cells in our network when the inputs are normal, while the filled bar shows the Pyr frequency when inputs are modulated. *Bii*: frequency of Pyr cells considered active (see METHODS). *C*: raster plots show Pyr cell activity when the network is fed by either unmodulated (*left*) or modulated (*right*) inputs. The odor is applied during the total extent of each simulation.

inal memories used during training, but with very low sparseness (~0.2) and synchronization (~0.3). The percentage of correct recalls was then determined. We considered as a correct recall every evoked activity M′ whose similarity (dot product described in *Eq. 9*) to the "pure" version of memory M was higher than the similarity of M′ to any other odor pattern stored in the network memory. We define the "pure" memory as the activation evoked in a network trained with one single memory. The results are shown in Fig. 9*A*. For a small number of odor memories, PC networks were able to correctly recall memories trained under both low- and high-sparseness conditions. As the number of memories increases, the success rate of networks trained with low-sparseness inputs quickly drops to close to zero. In contrast, networks trained with high-sparseness inputs can successfully recall a significantly higher number of memories. While input sparseness modulates the number of memories that can be simultaneously stored, input coherence during learning strongly affects the learning process per se, as illustrated in Fig. 9*B*. The graph shows the average synaptic weight of the top 50 strongest connections (Pyr-Pyr connections with higher *W*; see *Eq. 7* in METHODS for details) after subsequent sequences of 4-s training sessions. After a single training session, the average *W* trained with high-synchronization (coherence ~0.6) inputs jumps to ~0.22, while the weight in networks trained with low-synchronization inputs (coherence ~0.3) increases to around half of that (~0.11).

In summary, both Mi cell sparseness and coherence influence autoassociative learning. Mi sparseness affects memory capacity, while Mi coherence affects Pyr cell activation and learning rate.

Cholinergic Modulation in OB Improves Cortical Learning

The Pyr cell network exhibits more selective (fewer responsive cells) but stronger (responsive cells are more active) responses to odorants when ACh modulates the input coming from OB. Next, we tested how ACh modulation in the OB during learning affects the autoassociative memory function implemented by recurrent intrinsic connections between Pyr cells. In these simulations we used the full bulbar model.

We first trained the PC network to store a single, randomly chosen, pattern. Learning with (ON) and without (OFF) bulbar ACh was compared. After training for 7 s, the same odorant was presented to the network for recall, with ACh modulation OFF in both OB and PC. This process was repeated 50 times for statistical comparisons. After the learning process, the evoked activity in the Pyr cell network is influenced by both the Mi cell input and the input from intrinsic excitatory connections from other Pyr cells, strengthened during the learning process in an odor-specific pattern. The simulations show that the network trained with active cholinergic modulation in the OB evokes odor memories with significantly higher sparseness compared with those evoked before learning (Fig. 10*Ai*), indicating that learning renders the Pyr cells more selective to specific odorants. This increase in selectivity only happens in response to learning under cholinergic modulation.

The average pyramidal activity also shows a significant increase (Fig. 10*Aii*) from ~0.48 to ~1.0 Hz ($P < 0.001$) after learning with modulated inputs, as does the activity of odor-responsive neurons (Fig. 10*Aiii*), for which the average frequency increased from ~1.8 to ~4.9 Hz ($P < 0.001$). The coherence between PC cells did not show any significant change, remaining high in both scenarios (C ~0.85). We

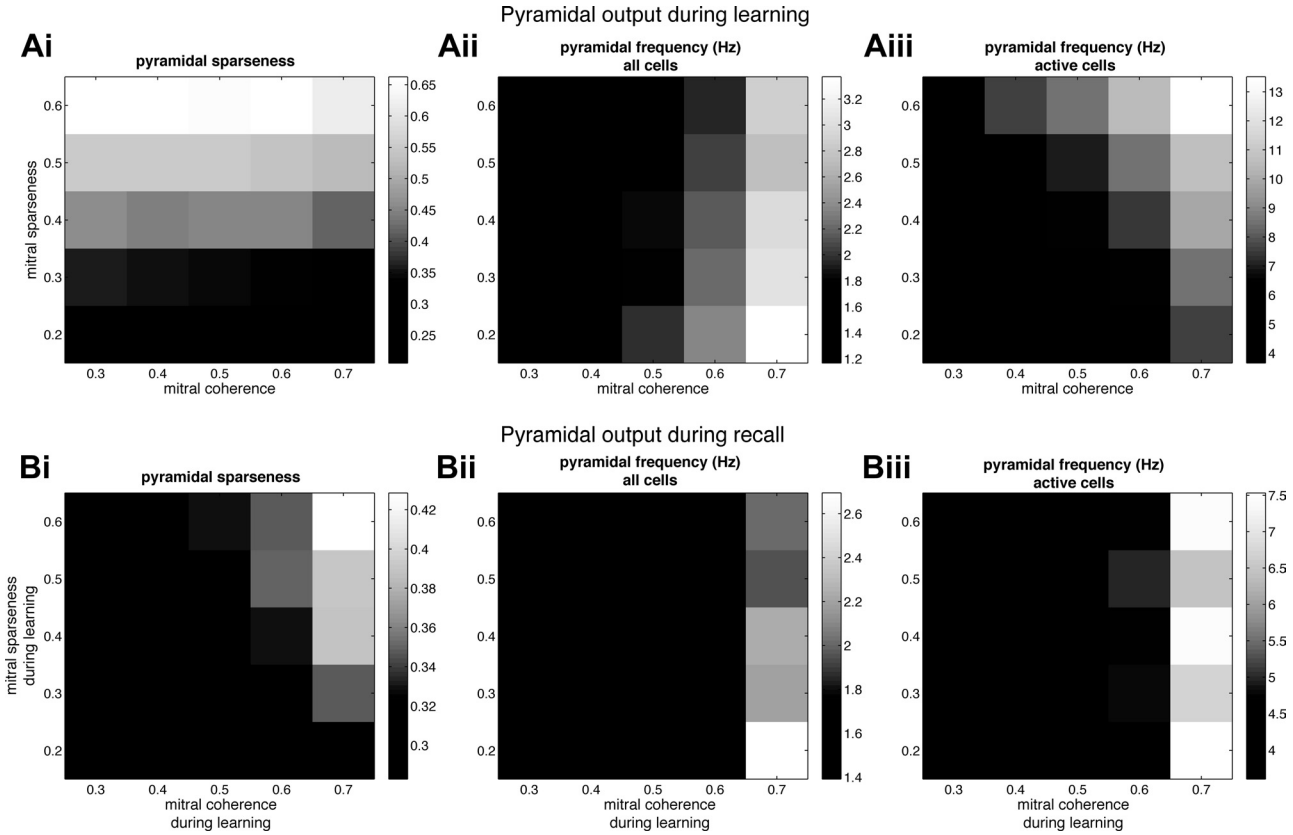

Fig. 8. Input sparseness and coherence play different roles in Pyr activation. *A*: input sparseness is directly related to Pyr sparseness, while input synchronization influences Pyr activity during learning; *x*- and *y*-axes represent variation in coherence and sparseness, respectively, of the PC inputs. *Ai*: increasing Mi sparseness strongly affects Pyr sparseness as well; the same impact is not observed when we vary Mi coherence. *Aii*: changes in input synchronization drastically impact Pyr cell activity; the effects of sparseness on Pyr frequency, however, are subtler. *Aiii*: when only cells considered active are taken into account, both sparseness and synchronization are important. The combination of sparse and coherent inputs increases the contrast between active and inactive cells (see text for reasoning). *B*: the combination of sparseness and coherence during learning influences sparseness, contrast, and firing frequency of recalled memories. Here we used inputs with low sparseness and coherence to recall the learned memories, similar to Fig. 7*A*. Therefore, the values in the *x*- and *y*-axes are levels of coherence and sparseness during the learning phase. *Bi*: the level of sparseness during learning directly impacts the sparseness in the recalled memory, while the input coherence seems to play a smaller role. *Bii*: Pyr cell activation during recalling is directly influenced by the level of input coherence during learning. However, memories with low input sparseness during learning show higher average frequency, indicating that input sparseness during learning also has some impact. *Biii*: the frequency of cells considered active during recall depends entirely on the level of input coherence during learning. The combined effect shown in *Bii* and *Biii* indicates that Mi synchronization might be crucial to improving learning and Pyr activation while the input sparseness can improve the noise-to-signal ratio.

therefore conclude that the higher learning rate in response to modulated inputs (shown in Fig. 10*Bii*) is due to the higher frequency of Pyr cells and not to higher synchronization. If we remove the connections between Pyr cells, the sparseness, overall frequency, and frequency of active cells drop to levels similar to before training (~0.47, 0.41 Hz, and 1.48 Hz, respectively), showing that these changes are in fact due to the strengthening of association fibers during the learning process.

We also sought to investigate how the similarity between two different odor representations in the Pyr network changed after learning. Figure 10*Aiv* shows that the similarity (*Eq. 9*) of two Pyr network outputs decreases as the similarity between Mi inputs is gradually reduced. This reduction, however, is significantly more pronounced in cases where the network was trained with modulated inputs. Training with unmodulated networks, in contrast, does not improve cortical discrimination.

Training with activated bulbar ACh leads to sparser yet stronger memory patterns in the PC network that are less overlapping. On the other hand, training the network without bulbar ACh did not cause any significant increase in selectivity or activation of Pyr cells or overlap. In summary, learning was more specific and the recalled pattern was stronger when trained with modulated inputs.

The difference between learning with or without bulbar ACh is also evident when we observe the dependence of Pyr activity on Mi cell synchronized firing. Figure 3 shows that in the naive network the Pyr cell activity depends on the coactivation of ~4+ Mi cells. In Fig. 10*Bi* we see that, after training the network to a given odorant pattern, the number of pyramidal spikes that depend on synchronized mitral spikes is reduced (white bars are the same results presented in Fig. 3*A*). This change, however, is more pronounced after the network learned from a mitral input modulated by ACh. Figure 10*Bii* shows that synaptic weights in networks trained with modulated inputs grow faster. After one training session, the average W in networks trained with modulated inputs increased to ~0.15, while the versions without modulated inputs during training increased to ~0.05. To reach the similar weight obtained after one session using modulated input, one needs no less than four 7-s training sessions with the unmodulated version. The dependence on synchronized Mi firing is reduced because after learning the cellular activity relies more on the

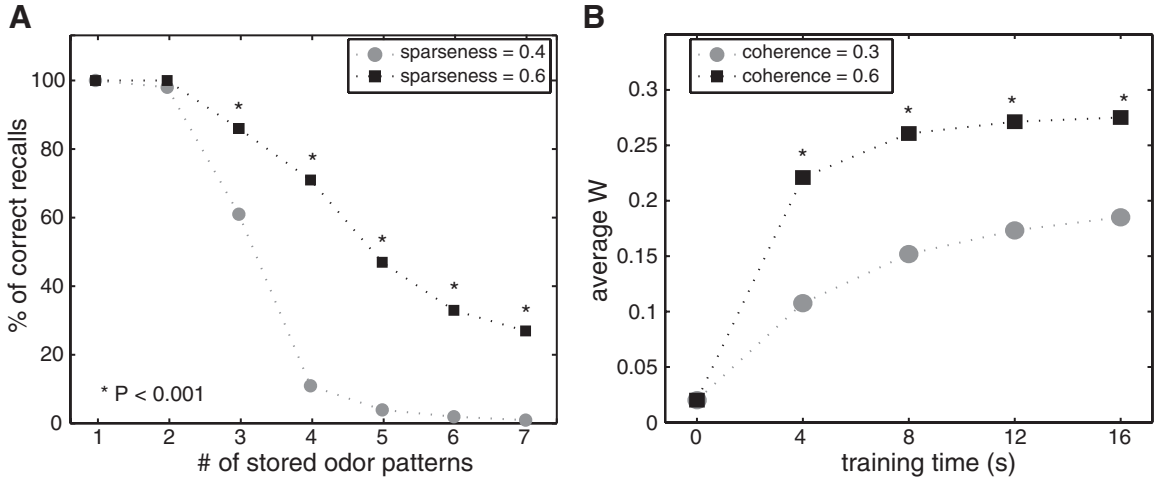

Fig. 9. Input sparseness impacts memory capacity and coherence impacts learning rate in Pyr networks. *A*: networks were trained to store groups of different odor memories presented sequentially. One group of networks was trained with low-sparseness odor inputs and another with high-sparseness inputs; coherence was kept constant. Networks trained with sparser odor inputs were able to correctly recover (see text for the criteria for correct recovery), on average, a larger number of stored memories than networks with low-sparseness odor inputs during training. *B*: Pyr networks receiving inputs with high coherence but equal sparseness learn faster. Graph shows the average weight (W) of the 50 strongest connections in Pyr networks trained with different levels of Mi synchronization; all other features were kept constant (sparseness ~0.6 and frequency ~8 Hz).

recurrent synapses than on afferent bulbar inputs. Consequently, the cortical network is more robust to changes in the signal-to-noise ratio in bulbar representations. Cortical representations created from modulated bulbar input respond more robustly to unmodulated input than those created from unmodulated input.

Memory Recovery Is More Efficient When Cortical Network Was Trained with ACh-Modulated Inputs

To test how PC network associative memory responds to corrupted input patterns, we trained 50 different networks with a random odor and then tried to recover the memory with a corrupted input pattern (Fig. 10*C*). The corruption levels in Fig. 10*C* are obtained by adding an increasingly large perturbation to OSNs' affinity to a given odorant. This perturbation was implemented as a random value n, where $-A \leq n \leq A$ and A is a percentage of the maximum affinity. To avoid negative or excessively high affinities the new affinity distribution was then normalized between zero and the max affinity value (see METHODS for details). For the results shown in Fig. 10*C*, we started with zero perturbation and gradually increased it in intervals of 4% of the max affinity (i.e., 0%, 4%, 8%, etc.). The input error in the x-axis is measured as the dissimilarity (calculated as $1 - D$, from *Eq. 9*) between the original and corrupted input, where 0 and 1 indicate, respectively, absolute identical and completely different inputs. We then measured the pairwise overlap between the evoked pattern, using the corrupted input and the memory evoked by the originally stored pattern (no error); this comparison was done in networks initially trained with bulbar ACh ON or OFF (Fig. 10*C*). With input error = 0, the output similarity evoked in Pyr cells trained with modulated inputs is significantly higher than that evoked in networks trained with bulbar ACh OFF, dropping from 0.96 to 0.84 ($P < 0.001$). This shows that in the absence of input error a cortical network trained with modulated inputs is more robust to the noise in spike patterns than a network trained with unmodulated inputs. Retrieval of memories trained using bulbar ACh ON is significantly better for a wide range of input errors, indicating that the network trained with modulated inputs is more robust to noise in incoming spike patterns.

Memories Trained with ACh-Modulated Inputs Are Recalled Better from Lower-Odor-Concentration Stimuli

We next investigated how the learned memories in the Pyr network are recalled when the network is exposed to a lower concentration of the learned odor. Initially, we used the same procedures adopted in Fig. 7. The Pyr cell network was trained with OB inputs with or without ACh modulation with the original overall input activation (1.0). After learning, the network was set to recall lower-concentration variants of the learned odorants. During the recall period, ACh was OFF. The concentration variants were implemented by reducing the current injection to all OSNs by a fixed fraction (see METHODS for reasoning about odor input patterns). Figure 11*A* shows the effect of gradually lower concentrations on sparseness of odor representation in Pyr cells. Note that when concentration is changed, sparseness is affected because the spatial distribution of activity changes. Additionally, coherence drops with decreasing concentration because the feedback loop between Mi and Gr cells is less active (when concentration was dropped to 50%, coherence changed from 0.63 to 0.31 under otherwise identical conditions). Sparseness is significantly higher in networks previously trained with modulated OB inputs for concentrations down to 0.4 of the trained concentration. Figure 11, *B* and *C* show that the overall Pyr frequency and the frequency for cells considered active are also significantly higher in networks trained with OB modulation ON. The gradual decrease of Pyr average activity is due to two reasons: *1*) the reduction of OSN and, consequently, Mi cell activity (Fig. 11, *B* and *C*) and *2*) furthermore, this lower activation of Mi cells leads to a lower activation of Gr cells (that depend on Mi activation) and lower synchronization, as shown in Fig. 4*B*. For example, if we drop concentration from 1.0 to 0.5, the Mi coherence drops from 0.68 to 0.31 ($P < 0.001$). It is interesting to note in Fig. 11*D* that the pairwise overlap (similarity) in the

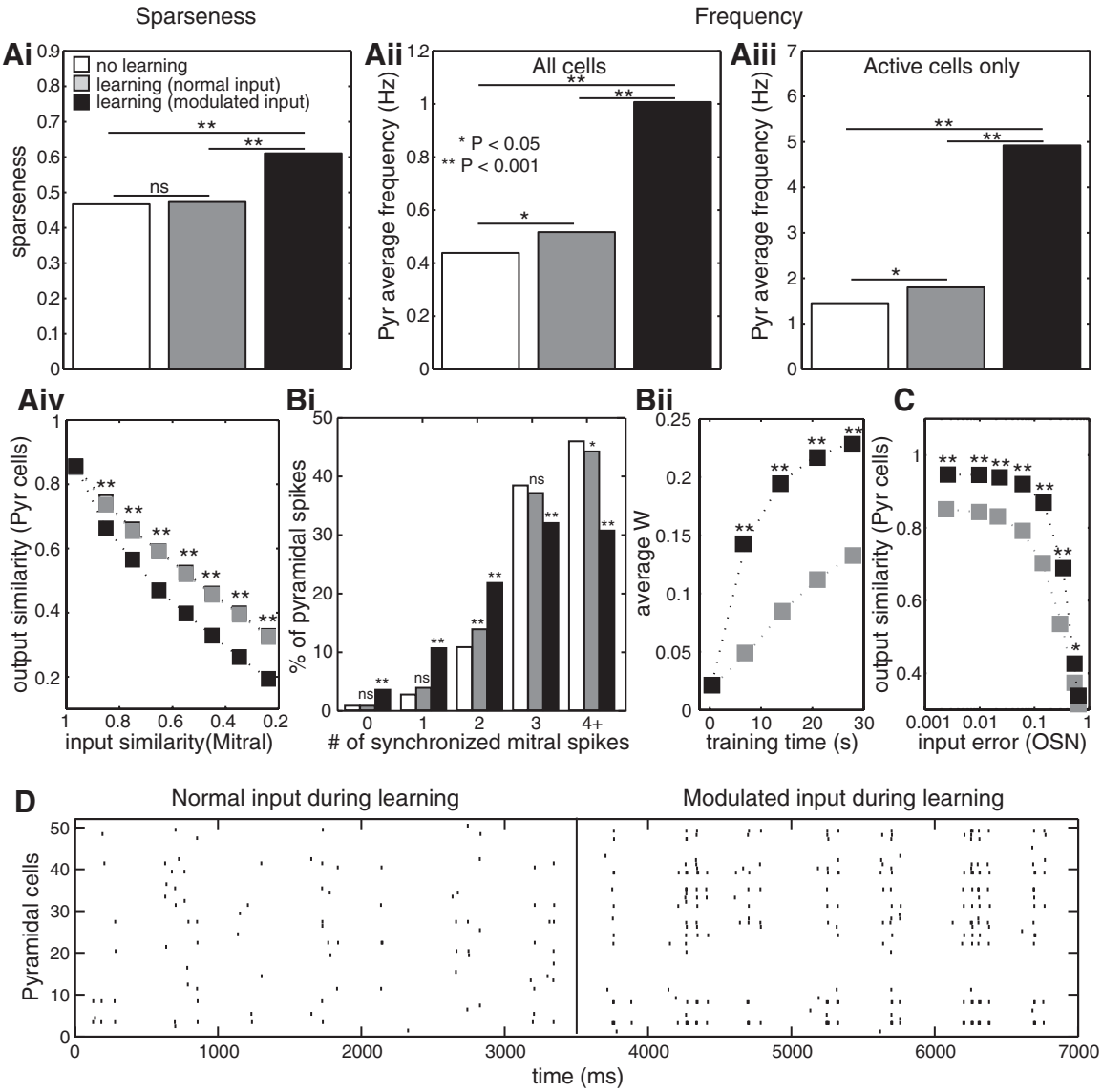

Fig. 10. ACh-modulated inputs during training increase average sparseness and firing frequency of Pyr cells, and error correction is also improved. *Ai*: sparseness in Pyr cell odor responses. Graph shows how the level of sparseness changes during recall of odor memories (ACh OFF) in 3 cases: no learning, training the network with unmodulated inputs from OB, and training the network with modulated inputs. During recall, we can see a significant increase in the average sparseness of Pyr cell network after training the recurrent connections for 7 s with ACh modulation in the bulb. If cholinergic modulation is absent in the bulb, there is no significant increase of sparseness compared with an untrained network. Similar to *Ai*, the average activity also increases when we measure the whole network activity (*Aii*) or only Pyr cells considered active (*Aiii*). *Aiv*: training memories with modulated inputs results in more dissimilar recalled memories. Akin to Fig. 5*Bii*, graph shows the similarity (*Eq. 9*) of 2 Pyr outputs in response to 2 different odorants (*y*-axis) as a function of the similarity between Mi inputs (*x*-axis). This test was repeated with 3 different scenarios: no learning (white), learning with unmodulated inputs (gray), and learning with modulated inputs (black). In these tests, the different odors were trained in different instances of the same network; therefore the synaptic weights of one memory are not influencing the activation of the other (for tests involving memory capacity and storage of multiple memories, see Fig. 9*A*). Graph shows that as the similarity between Mi inputs decreases the similarity between Pyr outputs also decreases, but this reduction is significantly more pronounced in examples where the network was trained with modulated inputs (**$P < 0.001$ modulated vs. no learning and modulated vs. unmodulated). The levels of similarity in examples with no training and training with unmodulated inputs show no significant difference and basically overlap each other. *B*: cholinergic modulation in the bulb increases the role of autoassociative connections between Pyr cells in PC. *Bi*: % of Pyr cells spikes that depended on 0, 1, 2, 3, and 4 or more presynaptic Mi cell synchronized spikes. White bars indicate % in simulations where no learning was applied. Gray and black bars show simulations where the Pyr network was trained with unmodulated and modulated inputs, respectively. After learning, Pyr cells spikes are less dependent on synchronized Mi activity since the network activity also relies on the excitatory Pyr-Pyr connections. The effect is enhanced when the network was trained while OB cholinergic modulation was ON. *Bii*: networks trained with modulated input also learn faster. Graph shows average weight (W) of the 50 strongest connections in Pyr networks trained with ACh ON or OFF. Before training, the average W is close to 0.02. After one 7-s training session, the average W in networks trained with modulated inputs increased to 0.15, while the versions without modulated inputs during training increased to 0.05. In fact, average weights in these networks only reached average W of ~0.15 after four 7-s training sessions. *C*: cholinergic modulation in OB improves error correction in the PC network. Graph shows similarity between memories recalled from uncorrupted and corrupted patterns as a function of corruption levels. Increasing the input error reduces the similarity in Pyr cell activity patterns with the pattern evoked by the stored input (output similarity, *y*-axis; see text for reasoning). Memories stored from ACh-modulated inputs were able to significantly better recover corrupted inputs for errors up to 0.1 compared with networks trained with unmodulated OB inputs. *D*: raster plots show difference in pyramidal activity after use of normal (*left*) or modulated (*right*) inputs during training. Compare to activity before training shown in Fig. 7*C*. In these figures, the odor was applied during the total extent of each simulation.

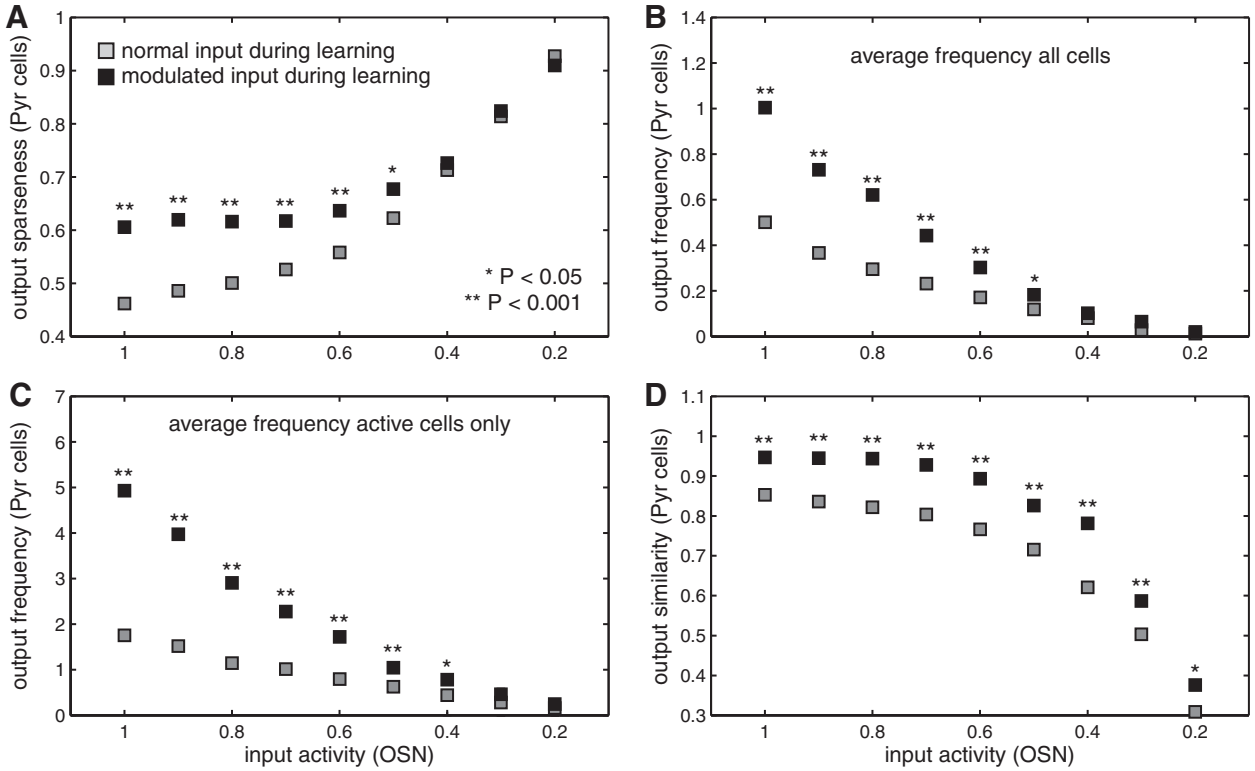

Fig. 11. Cholinergic modulation improves recall of odors presented at lower concentrations. *A*: odor contrast: networks trained with modulated input show significantly higher contrast (sparseness) for a wide range of concentration (represented here by overall input activation, see text). Graph shows an increase in average sparseness as we reduce the odor concentration as a consequence of the overall reduction of pyramidal activity. *B* and *C*: frequency: graphs show how frequency varies with odor concentration. Lowering odor concentration leads to a reduction of both the average Pyr cell activity as well as the frequency of cells considered active. However, the overall Pyr frequency and the frequency of odor-responsive cells considered active are also significantly higher in networks trained with OB modulation. *D*: recall: graph shows how the similarity between the memory evoked by the originally stored pattern (with activation = 1.0) and the memory recalled in response to lower concentrations changes as we reduce the odor concentration. For each concentration, the simulations were repeated 50 times with different odorants.

range of concentration between 1.0 and 0.4 is fairly constant and high, particularly for the cases where the network was trained with modulated inputs, indicating that, despite the lower frequency, the original odor pattern is well preserved.

One can also observe that the average sparseness in both tests increases as we lower the concentrations (Fig. 11*A*). This phenomenon is a consequence of the overall reduction of Pyr activity that leads to a reduction in the number of cells representing a given odor.

In summary, PC networks trained with modulated OB inputs are more robust to changes in concentration and can recall memorized patterns from low-concentration inputs.

DISCUSSION

Cholinergic modulation in the OB increases PG and Mi cell excitability, as well as Gr cell afterdepolarization. In the PC, ACh suppresses synaptic transmission in the Pyr cell autoassociative network and promotes LTP between these synapses. Previous computer models have tackled the possible roles of ACh modulation in one of the olfactory regions or specific neuronal subgroups (Hasselmo and Barkai 1995; Liljenstrom and Hasselmo 1995; Linster and Gervais 1996; Linster and Hasselmo 1997, 2001; Mandairon et al. 2006). Here we offer a broader model of the olfactory system and investigate how ACh modulation in these different parts combines to modulate olfactory memory. We find that cholinergic modulation of bulbar odor representations facilitates odor memory storage and recall in the cortical network by providing sparser and more synchronized inputs to the cortical network. As a result, stored cortical representations become more selective and more robust to degradation and noise.

Figure 12 summarizes our results. In our simulations, ACh improves contrast and synchronization in Mi cell output (Fig. 5, *Bi* and *Ci*). Each of these effects is derived from distinct neuronal interactions: *1*) In the glomerular layer, we use the concept of nontopographical contrast enhancement proposed by Cleland and Sethupathy (2006) and show that the increased excitability due to cholinergic modulation in PG cells results in the sharpening of the Mi cell odorant receptive field (Fig. 4*A* and Fig. 5*B*). *2*) The improvement in synchronization of Mi cell output, on the other hand, results from higher activation of Gr cells (Fig. 4*B* and Fig. 5*C*). The idea of Gr cell layer modulating spike synchronization in the OB has already been explored in previous models (Lagier et al. 2004; Schild 1988; White and Kauer 2001). It is interesting to observe that blocking muscarinic receptor in the modeled Gr cells (effectively turning OFF ACh modulation in these cells) has a relatively small impact on Mi cell sparseness while drastically reducing synchronization (Fig. 4*B* and Fig. 6). The equivalent of blocking nicotinic receptors in our simulations shows a significant reduction of Mi sparseness from ~0.53 to ~0.47 ($P < 0.001$; Fig. 6). These results are in accordance with Mandairon et al.

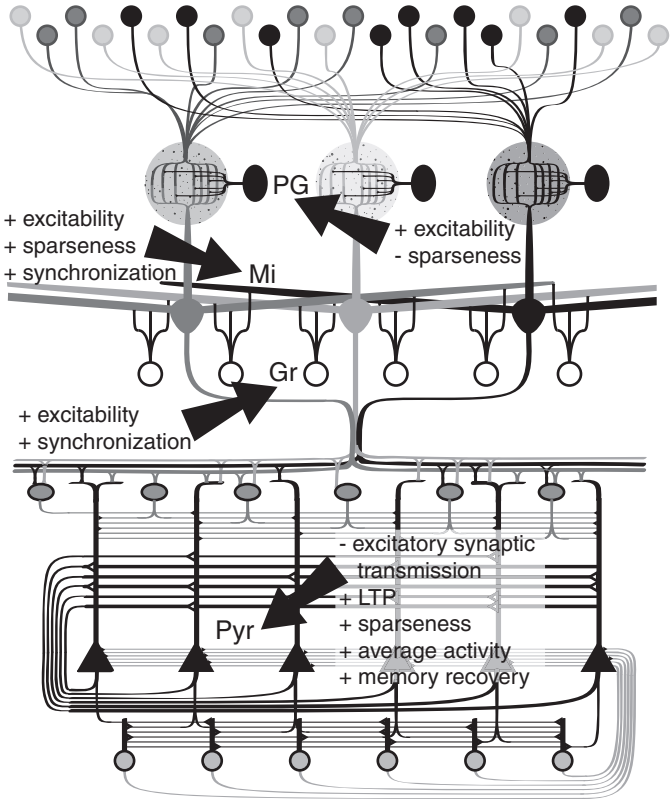

Fig. 12. Summary of ACh modulation in the model. ACh affects PG and Mi cell excitability; it also increases Gr cell afterdepolarization. Our model shows that this modulation increases contrast and synchronization of Mi cell output. In the PC, ACh suppresses excitatory transmission between Pyr cells but promotes long-term potentiation (LTP) between these synapses. Simulations presented here demonstrate an increase in sparseness (contrast) and average neuronal activity when the Pyr network was trained with modulated inputs from the bulb. Furthermore, the network also recovers corrupted memories better than when training used ACh OFF inputs, demonstrating more robust learning.

(2006), where the authors report relatively smaller impairments in odor discrimination when blocking muscarinic receptors compared with nicotinic blockage. The smaller muscarinic impact on sparseness, however, does not contradict the idea of contrast enhancement as a product of lateral inhibition mediated by Mi cell lateral dendrites (Davison et al. 2003; Migliore and Shepherd 2008; Schild 1988; Urban 2002) but rather indicates a more nuanced and complex network interaction regarding odor discrimination in the OB, with Gr cell layer contrast mediated by changes in synchronization rather than rate. Bulbar behavioral pharmacology experiments directly point to a role for nicotinic receptor modulation (PG and Mi cells) in decorrelation of similar odorants (Mandairon et al. 2006); however, in vivo recordings from Mi cells show that greater decorrelation in the OB due to elevated cholingeric modulation was impaired by blockade of nicotinic (PG and Mi cells) as well as muscarinic (Gr cells) receptors (Chaudhury et al. 2009). These data suggest an involvement of Gr cell modulation in modulation of contrast, as seen in our simulations and proposed by others (Davison et al. 2003; Migliore and Shepherd 2008; Schild 1988; Urban 2002), albeit not strong enough to be easily measurable in behavioral paradigms such as spontaneous or reward-driven discrimination (Chaudhury et al. 2009; Mandairon et al. 2006). Behaviorally, effects of cholinergic modulation are more difficult to measure in a reward-driven task (Chaudhury et al. 2009; Mandairon et al. 2006); this may be due to the fact that animals generally are easily trained to discriminate odorants in a reward-driven task that they do not spontaneously discriminate (Linster et al. 2002), possibly because reward-driven learning activates additional modulatory inputs that may compensate for the blockade of cholinergic receptors. The overall effects of cholinergic modulation on odor responses that we observe are in good agreement with results from a recent experiment using optogenetic techniques to directly stimulate cholinergic neurons in the HDB: PG and Gr cell sparseness decreases, whereas Mi sparseness increases (Ma and Luo 2012). The reported effects on spontaneous activity, different from those on odor-evoked activity, were not modeled here.

In the PC, ACh modulation suppresses synaptic transmission in the Pyr cell autoassociative network and promotes LTP between these synapses, indicating that cholinergic modulation could help to switch the system between training (ACh ON) and recovering (ACh OFF) modes (Linster and Hasselmo 2000, 2001; Linster et al. 2003). The reports from Davison and Ehlers (2011) show that Pyr cell firing depends on the coactivation of many glomeruli, indicating the importance of synchronized input. As expected, our model shows that feeding the PC with more synchronized (ACh ON) Mi inputs significantly increases Pyr cell activity, even if we keep the average input frequency the same (~4.0 Hz for ACh ON or OFF; see RESULTS for details), as shown in Fig. 7*B*. Not only are Pyr cells more active, but the neuronal selectivity is also improved. We observe higher sparseness when the Pyr network was trained with modulated inputs from the bulb (Fig. 7*A*).

A closer look in the sparseness and coherence of Mi outputs shows that Pyr network sparseness is directly dependent on the sparseness of its inputs while the average firing frequency depends on the coherence (Fig. 8*A*). High input coherence improves not only Pyr activation but also learning (Fig. 9*B*). Memories trained with high-coherence inputs showed a stronger activation during recall. Input sparseness, on the other hand, helps to increase the noise-to-signal ratio of odor representation before and after learning (Fig. 8, *A* and *B*). Input sparseness also affects memory capacity (Fig. 9*A*): the sparser and more decorrelated the input patterns to cortex, the higher the capacity of the cortical network under otherwise identical conditions.

Our simulations also show that the process of learning new odor patterns in Pyr network is improved by bulbar cholinergic modulation. Memories trained from modulated inputs are subsequently recovered with higher contrast and frequency (Fig. 10*A*) and also learned faster (Fig. 10*Bii*) than counterparts trained with unmodulated inputs. This improved recall indicates stronger synaptic weights between Pyr cells responding to the same odor pattern. The stronger weights make Pyr cells spikes less dependent on synchronized Mi activity since the Pyr network activity relies on the autoassociative connections (Fig. 10*Bi*).

Memories stored in the PC network under cholinergic modulation are most robust to pattern degradation, in both stimulus quality and concentration (Fig. 10*C* and Fig. 11). Memories trained with modulated inputs recovered from changes in odor quality significantly better than memories with normal OB inputs. Changes in odor concentration of modulated patterns

are recalled better in memories trained with modulated input than those of unmodulated patterns. Figure 11 shows that training odor memories with modulated input improves contrast (Fig. 11*A*), neuron frequency (Fig. 11, *B* and *C*), and similarity to the original memory (Fig. 11*D*) for a wide range of concentrations. Consequently, previously learned odorants can be recognized when present at significantly lower concentrations and changes in bulbar representations due to concentration (Cleland et al. 2007) can be counteracted in PC.

Our model makes a number of simplifications with respect to circuitry and function of olfactory bulb and cortex. First, several cell types are not included in both networks, such as short axon, external tufted, Blanes, and deep short axon cells in the OB, and deeper-layer Pyr cells and interneurons in olfactory cortex (Shepherd 1998). To date it is not known how these cell types are affected by cholinergic modulation, and hence it cannot be excluded that they would affect the results presented here. Similarly, we have simplified our neurons in such a manner that some known effects of ACh, such as changes in afterhyperpolarization, for example, cannot be represented. Details of temporal modulation of action potentials are not included, which have been suggested to carry information about odor quality in the OB (Cury and Uchida 2010; Shusterman et al. 2011). In the model presented here we have hence neglected fine temporal structures of Mi cell spiking within Mi cells connected to the same parent glomerulus (Dhawale et al. 2010) as well as between glomeruli and implemented only synchronization patterns between odor-responsive cells. The results we show are informative about the effects of cholinergic modulation on broad spiking activity and its impact on learning over several seconds of simulation time. Because the model focuses on how bulbar representations modify cortical processing, we have not yet implemented cortical feedback onto the bulb, known to undergo plasticity (Gao and Strowbridge 2009) and suggested to play a significant role in bulbar dynamics (Brea et al. 2009; Martin et al. 2004).

Within the limitations discussed above, the results presented here show that cholinergic modulation in both structures acts to change OB inputs to the cortex while modulating cortical associative memory function, ensuring that odor representations stored by the cortical network are sparse and robust to noise. More synchronized inputs to cortical neurons enhance synaptic plasticity by increasing cortical responses, while sparser inputs improve memory capacity. As a consequence of this, memories trained with modulated input are more robust to errors and lower-concentration inputs.

ACKNOWLEDGMENTS

The authors thank Sasha Devore and Guoshi Li for comments on the manuscript and Anuttama Sheela Mohan for suggestions in the model implementation code.

GRANTS

This work was supported by National Institute on Deafness and Other Communication Disorders Grant 1R01 DC-009948-01 to C. Linster; M. Idiart was supported by Brazilian agencies CNPq (305256/2008-4), Fapergs-Pronex (10/0008-10), and CAPES (0701-11-4).

DISCLOSURES

No conflicts of interest, financial or otherwise, are declared by the author(s).

AUTHOR CONTRIBUTIONS

Author contributions: L.B.d.A., M.A.P.I., and C.L. conception and design of research; L.B.d.A. performed experiments; L.B.d.A. analyzed data; L.B.d.A., M.A.P.I., and C.L. interpreted results of experiments; L.B.d.A. prepared figures; L.B.d.A. and C.L. drafted manuscript; L.B.d.A., M.A.P.I., and C.L. edited and revised manuscript; L.B.d.A., M.A.P.I., and C.L. approved final version of manuscript.

REFERENCES

Barkai E, Hasselmo ME. Modulation of the input/output function of rat piriform cortex pyramidal cells. *J Neurophysiol* 72: 644–658, 1994.

Bliss TV, Collingridge GL. A synaptic model of memory: long-term potentiation in the hippocampus. *Nature* 361: 31–39, 1993.

Brashear HR, Zaborszky L, Heimer L. Distribution of GABAergic and cholinergic neurons in the rat diagonal band. *Neuroscience* 17: 439–451, 1986.

Brea JN, Kay LM, Kopell NJ. Biophysical model for gamma rhythms in the olfactory bulb via subthreshold oscillations. *Proc Natl Acad Sci USA* 106: 21954–21959, 2009.

Buonviso N, Revial MF, Jourdan F. The projections of mitral cells from small local regions of the olfactory bulb: an anterograde tracing study using PHA-L (*Phaseolus vulgaris* leucoagglutinin). *Eur J Neurosci* 3: 493–500, 1991.

Castillo PE, Carleton A, Vincent JD, Lledo PM. Multiple and opposing roles of cholinergic transmission in the main olfactory bulb. *J Neurosci* 19: 9180–9191, 1999.

Chaudhury D, Escanilla O, Linster C. Bulbar acetylcholine enhances neural and perceptual odor discrimination. *J Neurosci* 29: 52–60, 2009.

Cleland TA. Early transformations in odor representation. *Trends Neurosci* 33: 130–139, 2010.

Cleland TA, Johnson BA, Leon M, Linster C. Relational representation in the olfactory system. *Proc Natl Acad Sci USA* 104: 1953–1958, 2007.

Cleland TA, Linster C. Computation in the olfactory system. *Chem Senses* 30: 801–813, 2005.

Cleland TA, Sethupathy P. Non-topographical contrast enhancement in the olfactory bulb. *BMC Neurosci* 7: 7, 2006.

Cury KM, Uchida N. Robust odor coding via inhalation-coupled transient activity in the mammalian olfactory bulb. *Neuron* 68: 570–585, 2010.

Davison AP, Feng J, Brown D. Dendrodendritic inhibition and simulated odor responses in a detailed olfactory bulb network model. *J Neurophysiol* 90: 1921–1935, 2003.

Davison IG, Ehlers MD. Neural circuit mechanisms for pattern detection and feature combination in olfactory cortex. *Neuron* 70: 82–94, 2011.

de Almeida L, Idiart M, Lisman JE. Memory retrieval time and memory capacity of the CA3 network: role of gamma frequency oscillations. *Learn Mem* 14: 795–806, 2007.

De Rosa E, Hasselmo ME. Muscarinic cholinergic neuromodulation reduces proactive interference between stored odor memories during associative learning in rats. *Behav Neurosci* 114: 32–41, 2000.

De Rosa E, Hasselmo ME, Baxter MG. Contribution of the cholinergic basal forebrain to proactive interference from stored odor memories during associative learning in rats. *Behav Neurosci* 115: 314–327, 2001.

Dhawale AK, Hagiwara A, Bhalla US, Murthy VN, Albeanu DF. Non-redundant odor coding by sister mitral cells revealed by light addressable glomeruli in the mouse. *Nat Neurosci* 13: 1404–1412, 2010.

Erdi P, Grobler T, Barna G, Kaski K. Dynamics of the olfactory bulb: bifurcations, learning, and memory. *Biol Cybern* 69: 57–66, 1993.

Gao Y, Strowbridge BW. Long-term plasticity of excitatory inputs to granule cells in the rat olfactory bulb. *Nat Neurosci* 12: 731–733, 2009.

Grobler T, Erdi P. Dynamic phenomena in the olfactory bulb. *Acta Biochim Biophys Hung* 26: 61–65, 1991.

Hasselmo ME, Anderson BP, Bower JM. Cholinergic modulation of cortical associative memory function. *J Neurophysiol* 67: 1230–1246, 1992.

Hasselmo ME, Barkai E. Cholinergic modulation of activity-dependent synaptic plasticity in the piriform cortex and associative memory function in a network biophysical simulation. *J Neurosci* 15: 6592–6604, 1995.

Hasselmo ME, Bower JM. Cholinergic suppression specific to intrinsic not afferent fiber synapses in rat piriform (olfactory) cortex. *J Neurophysiol* 67: 1222–1229, 1992.

Hasselmo ME, Cekic M. Suppression of synaptic transmission may allow combination of associative feedback and self-organizing feedforward connections in the neocortex. *Behav Brain Res* 79: 153–161, 1996.

Hines ML, Morse T, Migliore M, Carnevale NT, Shepherd GM. ModelDB: a database to support computational neuroscience. *J Comput Neurosci* 17: 7–11, 2004.

Isaacson JS. Odor representations in mammalian cortical circuits. *Curr Opin Neurobiol* 20: 328–331, 2010.

Jensen O, Idiart MA, Lisman JE. Physiologically realistic formation of autoassociative memory in networks with theta/gamma oscillations: role of fast NMDA channels. *Learn Mem* 3: 243–256, 1996.

Lagier S, Carleton A, Lledo PM. Interplay between local GABAergic interneurons and relay neurons generates gamma oscillations in the rat olfactory bulb. *J Neurosci* 24: 4382–4392, 2004.

Li YR, Matsunami H. Activation state of the M3 muscarinic acetylcholine receptor modulates mammalian odorant receptor signaling. *Sci Signal* 4: ra1, 2011.

Li Z, Hopfield JJ. Modeling the olfactory bulb and its neural oscillatory processings. *Biol Cybern* 61: 379–392, 1989.

Liljenstrom H, Hasselmo ME. Cholinergic modulation of cortical oscillatory dynamics. *J Neurophysiol* 74: 288–297, 1995.

Linster C, Cleland TA. Cholinergic modulation of sensory representations in the olfactory bulb. *Neural Netw* 15: 709–717, 2002.

Linster C, Cleland TA. Configurational and elemental odor mixture perception can arise from local inhibition. *J Comput Neurosci* 16: 39–47, 2004.

Linster C, Cleland TA. Decorrelation of odor representations via spike timing-dependent plasticity. *Front Comput Neurosci* 4: 157, 2010.

Linster C, Gervais R. Investigation of the role of interneurons and their modulation by centrifugal fibers in a neural model of the olfactory bulb. *J Comput Neurosci* 3: 225–246, 1996.

Linster C, Hasselmo M. Modulation of inhibition in a model of olfactory bulb reduces overlap in the neural representation of olfactory stimuli. *Behav Brain Res* 84: 117–127, 1997.

Linster C, Hasselmo ME. Neural activity in the horizontal limb of the diagonal band of Broca can be modulated by electrical stimulation of the olfactory bulb and cortex in rats. *Neurosci Lett* 282: 157–160, 2000.

Linster C, Hasselmo ME. Neuromodulation and the functional dynamics of piriform cortex. *Chem Senses* 26: 585–594, 2001.

Linster C, Henry L, Kadohisa M, Wilson DA. Synaptic adaptation and odor-background segmentation. *Neurobiol Learn Mem* 87: 352–360, 2007.

Linster C, Johnson BA, Morse A, Yue E, Leon M. Spontaneous versus reinforced olfactory discriminations. *J Neurosci* 22: 6842–6845, 2002.

Linster C, Maloney M, Patil M, Hasselmo ME. Enhanced cholinergic suppression of previously strengthened synapses enables the formation of self-organized representations in olfactory cortex. *Neurobiol Learn Mem* 80: 302–314, 2003.

Linster C, Menon AV, Singh CY, Wilson DA. Odor-specific habituation arises from interaction of afferent synaptic adaptation and intrinsic synaptic potentiation in olfactory cortex. *Learn Mem* 16: 452–459, 2009.

Ma M, Luo M. Optogenetic activation of basal forebrain cholinergic neurons modulates neuronal excitability and sensory responses in the main olfactory bulb. *J Neurosci* 32: 10105–10116, 2012.

Mandairon N, Ferretti CJ, Stack CM, Rubin DB, Cleland TA, Linster C. Cholinergic modulation in the olfactory bulb influences spontaneous olfactory discrimination in adult rats. *Eur J Neurosci* 24: 3234–3244, 2006.

Marr D. Simple memory: a theory for archicortex. *Philos Trans R Soc Lond B Biol Sci* 262: 23–81, 1971.

Martin C, Gervais R, Hugues E, Messaoudi B, Ravel N. Learning modulation of odor-induced oscillatory responses in the rat olfactory bulb: a correlate of odor recognition? *J Neurosci* 24: 389–397, 2004.

McQuiston AR, Katz LC. Electrophysiology of interneurons in the glomerular layer of the rat olfactory bulb. *J Neurophysiol* 86: 1899–1907, 2001.

Migliore M, Shepherd GM. Dendritic action potentials connect distributed dendrodendritic microcircuits. *J Comput Neurosci* 24: 207–221, 2008.

Mombaerts P, Wang F, Dulac C, Chao SK, Nemes A, Mendelsohn M, Edmondson J, Axel R. Visualizing an olfactory sensory map. *Cell* 87: 675–686, 1996.

Nagayama S, Enerva A, Fletcher ML, Masurkar AV, Igarashi KM, Mori K, Chen WR. Differential axonal projection of mitral and tufted cells in the mouse main olfactory system. *Front Neural Circuits* 4: 120, 2010.

Nickell WT, Shipley MT. Neurophysiology of magnocellular forebrain inputs to the olfactory bulb in the rat: frequency potentiation of field potentials and inhibition of output neurons. *J Neurosci* 8: 4492–4502, 1988.

Ojima H, Mori K, Kishi K. The trajectory of mitral cell axons in the rabbit olfactory cortex revealed by intracellular HRP injection. *J Comp Neurol* 230: 77–87, 1984.

Patil MM, Linster C, Lubenov E, Hasselmo ME. Cholinergic agonist carbachol enables associative long-term potentiation in piriform cortex slices. *J Neurophysiol* 80: 2467–2474, 1998.

Poo C, Isaacson JS. Odor representations in olfactory cortex: "sparse" coding, global inhibition, and oscillations. *Neuron* 62: 850–861, 2009.

Pressler RT, Inoue T, Strowbridge BW. Muscarinic receptor activation modulates granule cell excitability and potentiates inhibition onto mitral cells in the rat olfactory bulb. *J Neurosci* 27: 10969–10981, 2007.

Ravel N, Akaoka H, Gervais R, Chouvet G. The effect of acetylcholine on rat olfactory bulb unit activity. *Brain Res Bull* 24: 151–155, 1990.

Rolls ET, Tovee MJ. Sparseness of the neuronal representation of stimuli in the primate temporal visual cortex. *J Neurophysiol* 73: 713–726, 1995.

Schild D. Principles of odor coding and a neural network for odor discrimination. *Biophys J* 54: 1001–1011, 1988.

Schoenfeld TA, Knott TK. Evidence for the disproportionate mapping of olfactory airspace onto the main olfactory bulb of the hamster. *J Comp Neurol* 476: 186–201, 2004.

Shepherd GM. *The Synaptic Organization of the Brain*. New York: Oxford Univ. Press, 1998.

Shusterman R, Smear MC, Koulakov AA, Rinberg D. Precise olfactory responses tile the sniff cycle. *Nat Neurosci* 14: 1039–1044, 2011.

Stokes CC, Isaacson JS. From dendrite to soma: dynamic routing of inhibition by complementary interneuron microcircuits in olfactory cortex. *Neuron* 67: 452–465, 2010.

Treves A, Rolls ET. What determines the capacity of autoassociative memories in the brain? *Network* 2: 26, 1991.

Tseng GF, Haberly LB. Deep neurons in piriform cortex. II. Membrane properties that underlie unusual synaptic responses. *J Neurophysiol* 62: 386–400, 1989.

Urban NN. Lateral inhibition in the olfactory bulb and in olfaction. *Physiol Behav* 77: 607–612, 2002.

Wang XJ, Buzsaki G. Gamma oscillation by synaptic inhibition in a hippocampal interneuronal network model. *J Neurosci* 16: 6402–6413, 1996.

White J, Kauer JS. Exploring olfactory population coding using an artificial olfactory system. *Prog Brain Res* 130: 191–203, 2001.

Williams SH, Constanti A. A quantitative study of the effects of some muscarinic antagonists on the guinea-pig olfactory cortex slice. *Br J Pharmacol* 93: 855–862, 1988.

Wilson DA. Scopolamine enhances generalization between odor representations in rat olfactory cortex. *Learn Mem* 8: 279–285, 2001.

Zaborszky L, Carlsen J, Brashear HR, Heimer L. Cholinergic and GABAergic afferents to the olfactory bulb in the rat with special emphasis on the projection neurons in the nucleus of the horizontal limb of the diagonal band. *J Comp Neurol* 243: 488–509, 1986.